ER stress transcription factor Xbp1 suppresses intestinal tumorigenesis and directs intestinal stem cells

ER stress transcription factor Xbp1 suppresses intestinal tumorigenesis and directs intestinal stem cells

Lukas Niederreiter,[1] Teresa M.J. Fritz,[2] Timon E. Adolph,[1] Anna-Maria Krismer,[2] Felix A. Offner,[5] Markus Tschurtschenthaler,[2] Magdalena B. Flak,[6] Shuhei Hosomi,[6] Michal F. Tomczak,[6] Nicole C. Kaneider,[1,3] Edina Sarcevic,[5] Sarah L. Kempster,[1] Tim Raine,[1] Daniela Esser,[7] Philip Rosenstiel,[7] Kenji Kohno,[8] Takao Iwawaki,[9,10] Herbert Tilg,[3,4] Richard S. Blumberg,[6] and Arthur Kaser[1]

[1]Division of Gastroenterology and Hepatology, Department of Medicine, Addenbrooke's Hospital, University of Cambridge, Cambridge CB2 0QQ, England, UK
[2]Department of Internal Medicine II, [3]Christian Doppler Research Laboratory for Gut Inflammation, and [4]Department of Internal Medicine I, Innsbruck Medical University, A-6020 Innsbruck, Austria
[5]Department of Pathology, Academic Teaching Hospital Feldkirch, A-6800 Feldkirch, Austria
[6]Division of Gastroenterology, Hepatology, and Endoscopy, Department of Medicine, Brigham and Women's Hospital, Harvard Medical School, Boston, MA 02115
[7]Institut für Klinische Molekularbiologie, Christian-Albrechts-Universität zu Kiel, D-24105 Kiel, Germany
[8]Laboratory of Molecular and Cell Genetics, Nara Institute of Science and Technology, Ikoma, Nara 630-0192, Japan
[9]Advanced Scientific Research Leaders Development Unit, Gunma University, Maebashi, Gunma 371-8511, Japan
[10]Iwawaki Initiative Research Unit, Advanced Science Institute, Institute of Physical and Chemical Research, Wako, Saitama 351-0198, Japan

Unresolved endoplasmic reticulum (ER) stress in the epithelium can provoke intestinal inflammation. Hypomorphic variants of ER stress response mediators, such as *X-box–binding protein 1* (*XBP1*), confer genetic risk for inflammatory bowel disease. We report here that hypomorphic Xbp1 function instructs a multilayered regenerative response in the intestinal epithelium. This is characterized by intestinal stem cell (ISC) expansion as shown by an inositol-requiring enzyme 1α (Ire1α)–mediated increase in Lgr5$^+$ and Olfm4$^+$ ISCs and a Stat3-dependent increase in the proliferative output of transit-amplifying cells. These consequences of hypomorphic Xbp1 function are associated with an increased propensity to develop colitis-associated and spontaneous *adenomatous polyposis coli* (*APC*)–related tumors of the intestinal epithelium, which in the latter case is shown to be dependent on Ire1α. This study reveals an unexpected role for Xbp1 in suppressing tumor formation through restraint of a pathway that involves an Ire1α- and Stat3-mediated regenerative response of the epithelium as a consequence of ER stress. As such, Xbp1 in the intestinal epithelium not only regulates local inflammation but at the same time also determines the propensity of the epithelium to develop tumors.

CORRESPONDENCE
Arthur Kaser:
ak729@cam.ac.uk
OR
Richard S. Blumberg:
rblumberg@partners.org

Abbreviations used: AOM, azoxymethane; *APC*, *adenomatous polyposis coli*; CAC, colitis-associated cancer; CRC, colorectal cancer; DSS, dextran sodium sulfate; IBD, inflammatory bowel disease; IEC, intestinal epithelial cell; IHC, immunohistochemistry; ISC, intestinal stem cell; ISH, in situ hybridization; PCNA, proliferating cell nuclear antigen; ROS, reactive oxygen species; UPR, unfolded protein response.

Colorectal cancer (CRC) is the second most prevalent cause of death from cancer in the Western world (Lieberman, 2009). One third of the 147,000 patients diagnosed with CRC every year in the United States will succumb to the disease (Lieberman, 2009). Significant progress has been made in revealing somatic genetic alterations in CRC, ranging from the now classical adenoma–carcinoma sequence to insights into genomic instability and patterns of accumulation of somatic mutations at distinct genes and loci (Kinzler and Vogelstein, 1996; Cancer

L. Niederreiter and T.M.J. Fritz contributed equally to this paper.
R.S. Blumberg and A. Kaser contributed equally to this paper.
A. Kaser began work for this study at the Dept. of Internal Medicine II, Innsbruck Medical University, A-6020 Innsbruck, Austria.

The Rockefeller University Press $30.00
J. Exp. Med. 2013 Vol. 210 No. 10 2041-2056
www.jem.org/cgi/doi/10.1084/jem.20122341

The Journal of Experimental Medicine

Genome Atlas Network, 2012). Epidemiological studies support environmental factors such as obesity as being important in the pathogenesis of cancer, including CRC (Calle et al., 2003; Aggarwal et al., 2009).

CRC arises from the intestinal epithelium, a highly proliferative tissue which renews itself every several days under steady-state conditions. Upon intestinal epithelial injury and cell loss, such homeostatic renewal is supplanted by a regenerative response, which also represents an important defense strategy of the host (Amcheslavsky et al., 2009; Cronin et al., 2009; Jiang et al., 2009). However, an unabated regenerative, wound healing–like response to tissue injury may lay the ground for intestinal tumors (Kuraishy et al., 2011). This is clinically evident by the common occurrence of tumors at sites of chronic injury (e.g., colitis-associated cancer [CAC] in inflammatory bowel disease [IBD] or gastric cancer upon *Helicobacter pylori* infection). Hence, the remarkable paradox emerges that cell death caused by tissue injury augments the tumorigenic potential of adjoining cells (Kuraishy et al., 2011). Inflammatory signals from the chronically inflamed intestinal microenvironment, such as IL-6 and IL-11 among others, have been identified to contribute to such tumor-promoting activities in the injured intestine (Becker et al., 2004; Bollrath et al., 2009; Grivennikov et al., 2009).

In mammals, the intestinal epithelial compartment consists of several subtypes of differentiated cells (absorptive, Paneth, goblet, and enteroendocrine cells) that arise from rapidly cycling $Lgr5^+Olfm4^+$ intestinal stem cells (ISCs) at the crypt bottom (Barker et al., 2007). This $Lgr5^+$ stem cell population also gives continuous rise to a quiescent label-retaining population, located at the +4 position and expressing Lgr5, that is committed to mature into Paneth and enteroendocrine cells, but which can alternatively be recalled to the stem cell state within the crypt in instances of injury to the crypt (Sangiorgi and Capecchi, 2008; Montgomery et al., 2011; Takeda et al., 2011; Tian et al., 2011; Buczacki et al., 2013; Clevers, 2013). ISCs feed into transit-amplifying cells, which serve as the forerunners of the differentiated intestinal epithelial cell (IEC) types (Barker et al., 2007). Through a model of human sporadic and familial CRC, ISCs have been revealed as the cells of origin of intestinal cancer (Barker et al., 2009; Zhu et al., 2009; Schepers et al., 2012).

The unfolded protein response (UPR) is a cytoprotective response to ER stress that arises when misfolded proteins accumulate in this organelle (Schröder and Kaufman, 2005; Todd et al., 2008; Walter and Ron, 2011). In metazoans, three core UPR-associated pathways coordinate an adaptive response to ER stress that results in expansion of the ER, promotion of ER-associated degradation and chaperone functions and, when unabated, cellular death by apoptosis. The evolutionarily most conserved UPR branch consists of inositol-requiring enzyme 1α (Ire1α; encoded by *Ern1*), an ER stress sensor, and the transcription factor X-box–binding protein 1 (Xbp1) as its effector (Schröder and Kaufman, 2005; Ron and Walter, 2007; Todd et al., 2008; Kohno, 2010; Walter and Ron, 2011). Ire1α activates Xbp1 by conversion of unspliced Xbp1 (Xbp1u) mRNA to spliced Xbp1 (Xbp1s) via its atypical endoribonuclease function, which removes 26nt within Xbp1u to generate an alternate reading frame (Xbp1s; Hetz et al., 2011; Walter and Ron, 2011). Unresolved ER stress in IECs has emerged as an important mechanism that initiates inflammation in the intestine (Kaser et al., 2008). Specifically, partial or complete *Xbp1* deletion in mouse IECs leads to unresolved ER stress and consequently hypersensitivity of IECs to inflammatory and microbial signals, Paneth cell dysfunction with loss of their characteristic granules, increased epithelial apoptosis, spontaneous small intestinal enteritis, and increased susceptibility to colitis-inducing agents (Kaser et al., 2008). Fittingly, hypomorphic *XBP1* variants confer genetic risk for both forms of IBD, Crohn's disease and ulcerative colitis (Kaser et al., 2008). Additional genetic risk factors that impact the UPR have been discovered in IBD (e.g., *ORMDL3* [McGovern et al., 2010] and *AGR2* [Zheng et al., 2006]), and in some cases their genetic deletion in mice can lead to spontaneous IBD-like disease as well (Zhao et al., 2010). Notably, it appears that IECs in IBD generally experience unresolved ER stress, even in the absence of overt tissue-destructive inflammation (Heazlewood et al., 2008; Kaser et al., 2008; Tréton et al., 2011), with the effectiveness of the UPR being under the influence of primary (genetic) and secondary (environmental) factors (Kaser and Blumberg, 2011). Prompted by the increased turnover of IECs in mice that lack *Xbp1* (Kaser et al., 2008), here we investigated the UPR's role in epithelial regeneration and its implications for intestinal tumorigenesis.

RESULTS

Xbp1 deletion increases ISC numbers

The *Xbp1*-deficient small intestinal epithelium exhibits increased turnover (Kaser et al., 2008), which is similarly present in the colon (Fig. 1, A and B). A 2-h pulse of BrdU revealed expansion of the transit-amplifying zone in the ileum and colon, whereas a 24-h pulse demonstrated accelerated migration of IECs along the crypt–villus axis in IEC-conditional knockout $Xbp1^{-/-(IEC)}$ mice compared with $Xbp1^{+/+(IEC)}$ littermates (Fig. 1, A–C). This corresponded with increased numbers of proliferating cell nuclear antigen $(PCNA)^+$ cells along the crypt–villus axis in $Xbp1^{-/-(IEC)}$ mice (Fig. 1, D and E). Moreover, deletion of *Xbp1* resulted in a 57 ± 3% increase in $Olfm4^+$ ISCs (Fig. 1, F and G). This correlated with an increased number of $BrdU^+$ cells at the crypt base consistent with proliferating ISCs (Fig. 1 H). In situ hybridization (ISH) for Lgr5 indicated increased expression in $Xbp1^{-/-(IEC)}$ compared with $Xbp1^{+/+(IEC)}$, both in the small intestine and colon (Fig. 1 I). This was also reflected by a trend toward increased *Lgr5* mRNA expression in isolated crypts upon quantification by RT-PCR (Fig. 1 J) and significantly increased expression of characteristic mRNAs that define the ISC signature (Fig. 1 J; Sato et al., 2011; Muñoz et al., 2012). Altogether, these data indicate an expansion of ISC numbers in $Xbp1^{-/-(IEC)}$ compared with $Xbp1^{+/+(IEC)}$ mice. This increase in ISCs is interesting because Paneth cells, which contribute to the ISCs' niche to a variable extent depending on the model system studied

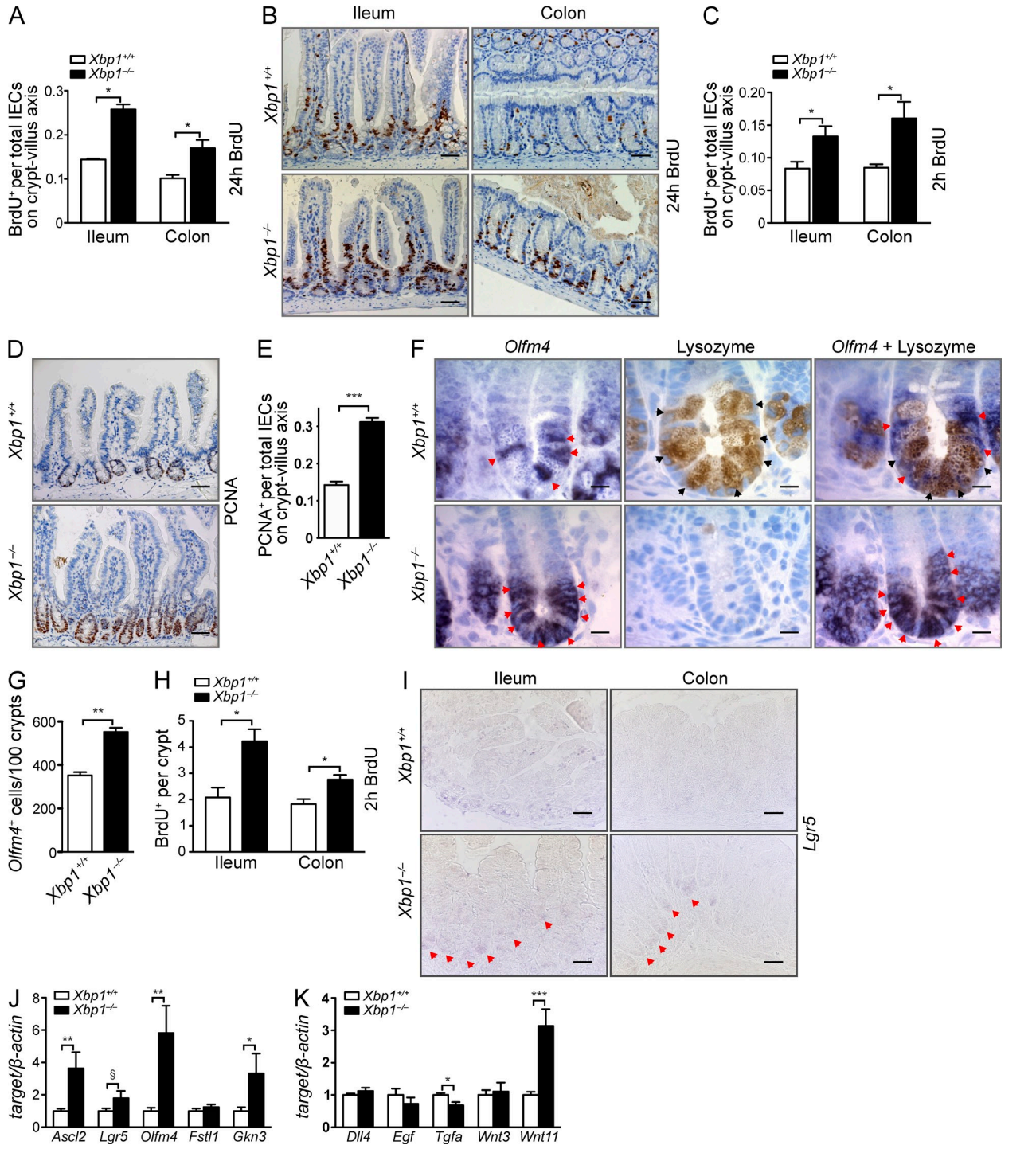

Figure 1. ***Xbp1*** **deletion increases ISC numbers.** (A) Animals were injected with BrdU and sacrificed 24 h later. BrdU$^+$ cells per total cells along the crypt–villus axis were counted (n = 3/4; two-tailed Student's t test). (B) Anti-BrdU IHC of the ileum and colon 24 h after i.p. injection with BrdU (n = 3/4). (C) Similar experiment as A with a 2-h BrdU pulse to assess transit-amplifying cells (n = 4/4; two-tailed Student's t test). (D) Anti-PCNA IHC of the small intestine (n = 5/5). (E) PCNA$^+$ cells per total cells along the crypt–villus axis were counted (n = 5/5; two-tailed Student's t test). (F) Olfm4$^+$ ISCs (ISH; red arrowheads) in the small intestine of *Xbp1*$^{+/+(IEC)}$ and *Xbp1*$^{-/-(IEC)}$ mice. Lysozyme staining identified fully differentiated Paneth cells (black arrowheads) intermingled with ISCs (n = 3/4). (G) Quantification of Olfm4$^+$ ISCs per 100 crypts (n = 3/4; two-tailed Student's t test). (H) Sections of *Xbp1*$^{+/+(IEC)}$ and *Xbp1*$^{-/-(IEC)}$ mice from C were analyzed for BrdU$^+$ cells at the crypt bottom up to position +4 (n = 4/4). (I) ISC identification by Lgr5 ISH in ileum and colon (Lgr5$^+$ crypts marked by red arrowheads; n = 4/4). Bars: (B, D, and I) 20 µm; (F) 5 µm. (J and K) Analysis of isolated crypt mRNA of *Xbp1*$^{+/+(IEC)}$ and *Xbp1*$^{-/-(IEC)}$ mice for transcripts representative of the ISC signature (J; Muñoz et al., 2012) or Paneth cell signature (K; Sato et al., 2011) by RT-pPCR (n = 12/11; Student's t test). Graphs show mean ± SEM. §, P = 0.0548; *, P < 0.05; **, P < 0.01; ***, P < 0.001.

(Sato et al., 2011; Durand et al., 2012; Kim et al., 2012; Yilmaz et al., 2012), are morphologically condensed to Paneth cell remnants that lack their characteristic secretory apparatus when *Xbp1* is deleted (Kaser et al., 2008). Among the genes that had been reported as most highly enriched in Paneth cells and that could support a niche function for ISCs are *Wnt3*, *Wnt11*, *Egf*, *Tgfa*, and *Dll4* (Sato et al., 2011). Among those, we noted a threefold increase in mRNA expression of *Wnt11* in $Xbp1^{-/-(IEC)}$ compared with $Xbp1^{+/+(IEC)}$ crypts (Fig. 1 K).

ISC expansion is dependent on overactivation of Ire1α

The design of the floxed *Xbp1* allele results in a premature stop codon upon Cre-mediated deletion of exon 2, but it retains the capacity to monitor the splicing status of *Xbp1* mRNA (Kaser et al., 2008). Reduced or absent Xbp1 function in IECs leads to profound splicing of *Xbp1* mRNA (Kaser et al., 2008), which is consistent with unresolved ER stress and indicative of massive Ire1α activation (Hetz et al., 2011). Indeed, although Ire1α phosphorylation was not detectable in $Xbp1^{+/+(IEC)}$ epithelium, *Xbp1* deletion resulted in strong Ire1α phosphorylation, along with increased expression of total protein (Fig. 2 A). To test whether Ire1α is involved in ISC activation under ER stress, we generated double-conditional $VCre;Ern1^{fl/fl};Xbp1^{fl/fl}$ mice. Fig. 2 (B and C) shows abrogation of the increase in ISC numbers in the small intestine of $Xbp1^{-/-(IEC)};Ern1^{-/-(IEC)}$ compared with $Xbp1^{-/-(IEC)};Ern1^{+/+(IEC)}$ mice, with $Xbp1^{-/-(IEC)};Ern1^{+/-(IEC)}$ mice exhibiting an intermediate phenotype. In contrast, under homeostatic conditions in *Xbp1*-sufficient IECs ($Xbp1^{+/+(IEC)}$), Ire1α did not affect the size of the ISC pool (Fig. 2 D). The floxed exons 20 and 21 of the *Ern1* allele encode the endoribonuclease domain of Ire1α, whereas the kinase domain is encoded upstream and remains intact (Iwawaki et al., 2009). In $Ern1^{-/-(IEC)}$ mice, a truncated Ire1α protein was detectable (Fig. 2 E) that lacked the capacity for massive Xbp1 mRNA splicing in *Xbp1*-deficient IECs of double mutant mice (Fig. 2 F), as expected, and indeed was not phosphorylated under ER stress, demonstrating loss of its endoribonuclease and kinase activity (Fig. 2 A). In addition to ubiquitously expressed Ire1α, IECs express another isoform (Ire1β) with the capacity to splice *Xbp1* mRNA (Bertolotti et al., 2001). It is therefore remarkable that genetic co-deletion of Ire1α ($Xbp1^{-/-(IEC)};Ern1^{-/-(IEC)}$) alone was sufficient to completely revert the massive splicing of *Xbp1* mRNA to the baseline levels observed in *Xbp1*-sufficient IECs (Fig. 2 F). This implies that Ire1β is not overactivated in a similar way as is Ire1α as a consequence of ER stress caused by Xbp1 deletion. Hence, Ire1α drives regenerative ISC expansion upon sensing ER stress in the intestinal epithelium, but it is not involved in homeostatic ISC regulation. In contrast to ISC expansion, Ire1α did not affect the hyperproliferation of the ER-stressed, *Xbp1*-deleted intestinal epithelium (Fig. 2 G). Collectively, these data indicate that although hyperproliferation and ISC expansion are both consequences of *Xbp1* deletion and presumably ER stress, only the increase in ISC numbers is under the control of Ire1α.

Hypomorphic Xbp1 leads to Jak1/Stat3 activation in IECs

In *Drosophila melanogaster*, injured enterocytes induce cytokines (*Upd*, *Upd2*, and *Upd3*) that activate Jak/Stat (*dome*, *hop*, and *STAT92E*) signaling in intestinal epithelial stem cells, which promotes their division and initiates progenitor cell differentiation (Amcheslavsky et al., 2009; Jiang et al., 2009). In the mammalian system, this feedback mechanism that links enterocyte loss to stem cell output is less well understood. The mammalian orthologues of the *Drosophila* pathway (IL-6, IL-11, and Stat3) play an important role in IEC regeneration (Becker et al., 2004; Bollrath et al., 2009; Grivennikov et al., 2009; Pickert et al., 2009). Fig. 3 A shows substantial levels of Stat3 Tyr-705 phosphorylation (p) in the $Xbp1^{-/-(IEC)}$ epithelium, whereas only minimal p-Stat3 was observed in $Xbp1^{+/+(IEC)}$ epithelium. Immunohistochemistry (IHC) localized p-Stat3 to the transit-amplifying zone with further extension into the villus epithelium, with barely any immunoreactivity demonstrable within the crypts (Fig. 3 B). Jak1 but not Jak2 phosphorylation was also induced in $Xbp1^{-/-(IEC)}$ compared with $Xbp1^{+/+(IEC)}$ epithelium (Fig. 3 A). Total Stat3 as well as Jak1 and Jak2 was also increased (Fig. 3 A), which might reflect the known capacity of Stat3 to bind its own promoter and to transactivate its transcription (Narimatsu et al., 2001; Lam et al., 2008; Snyder et al., 2008). Increased p-Stat3 was independent of Ire1α as $Xbp1^{-/-(IEC)};Ern1^{-/-(IEC)}$ and $Xbp1^{-/-(IEC)};Ern1^{+/+(IEC)}$ epithelia exhibited similar levels (Fig. 3 C). These experiments provide evidence for Ire1α-independent Stat3 activation in *Xbp1*-deficient epithelia that localizes to the transit-amplifying zone and its downstream progeny.

Stat3 blockade abrogates epithelial hyperproliferation in Xbp1-deficient epithelium

S3I-201 selectively inhibits Stat3 transcriptional activities by blocking dimer formation and DNA binding (Siddiquee et al., 2007). To test whether Stat3 is responsible for epithelial hyperproliferation in *Xbp1*-deficient IECs, we administered S3I-201 i.p. every other day for 14 d to $Xbp1^{-/-(IEC)}$ mice. Fig. 3 D demonstrates that Stat3 inhibition abrogated the increased turnover of the intestinal epithelium in $Xbp1^{-/-(IEC)}$ mice. Notably, S3I-201 did not affect ISC numbers in $Xbp1^{-/-(IEC)}$ mice (Fig. 3 E), which is consistent with an absence of p-Stat3 in crypts (Fig. 3 B). Of note, S3I-201 did not affect epithelial turnover in *Xbp1*-sufficient mice (not depicted), indicating that this Stat3-dependent mechanism is specifically engaged under conditions of ER stress. Altogether, these data establish that *Xbp1* deficiency results in Stat3 activation in the transit-amplifying zone, which mediates the hyperproliferation of ER-stressed IECs.

Hypomorphic Xbp1 induces an autocrine activation loop in IECs via NF-κB, IL-6/IL-11, and Stat3

We chose the small IEC line MODE-K as a model system for studying the mechanisms underlying Stat3 activation and silenced *Xbp1* expression via a lentivirus expressing a specific shRNA (Kaser et al., 2008). Stable *Xbp1* silencing resulted in profound Stat3 Tyr-705 phosphorylation compared with

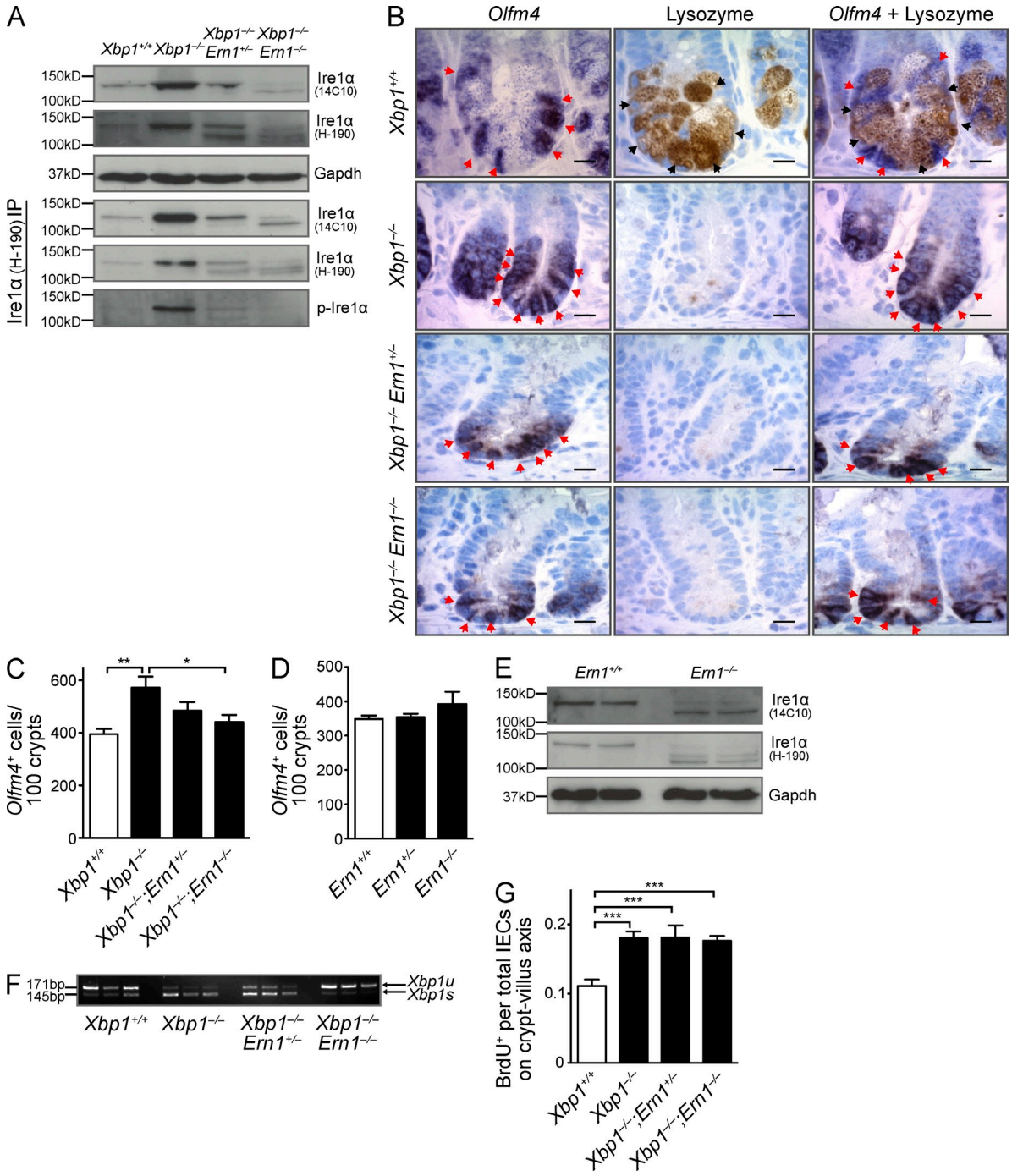

Figure 2. ISC expansion is dependent on overactivation of Ire1α. (A) Immunoblot of total and phosphorylated Ire1α of indicated genotypes in total epithelial scrapings or after immunoprecipitation (IP) as indicated. Samples were immunoprecipitated with anti-Ire1α pAb H-190 (immunogen: amino acids 371–560) and immunoblotted with anti-Ire1α mAb 14C10 (immunogen: C-terminal fragment) or pAb H-190. Data are representative of four independent experiments. (B) Sections of the indicated genotypes were in situ hybridized for Olfm4 (red arrowheads), stained for lysozyme (black arrowheads), or both ($n = 5$ per group). Bars, 5 µm. (C) Quantification of Olfm4$^+$ ISCs per 100 crypts ($n = 5$ per group with combined analysis of duodenum, jejunum, and ileum; one-way ANOVA with Bonferroni post-hoc test). (D) Quantification of Olfm4$^+$ ISCs in $Ern1^{+/+(IEC)}$, $Ern1^{+/-(IEC)}$, and $Ern1^{-/-(IEC)}$ mice ($n = 5$ per group). (E) Western blot of $Ern1^{+/+(IEC)}$ and $Ern1^{-/-(IEC)}$ (exons 20–21 floxed) mice immunoblotted with mAb 14C10 and pAb H-190 detects a truncated Ire1α protein in $Ern1^{-/-(IEC)}$ epithelial scrapings. (F) Xbp1 mRNA splicing in epithelial scrapings of the indicated genotypes. 171 bp, Xbp1u; 145 bp, Xbp1s. (E and F) Data are representative of two independent experiments. (G) Animals were injected with BrdU and harvested 24 h later to assess epithelial turnover. BrdU$^+$ cells per total cells along the crypt–villus axis were counted ($n = 4$ per group with combined analysis of duodenum, jejunum, and ileum; one-way ANOVA with Bonferroni post-hoc test). Graphs show mean ± SEM. *, $P < 0.05$; **, $P < 0.01$; ***, $P < 0.001$.

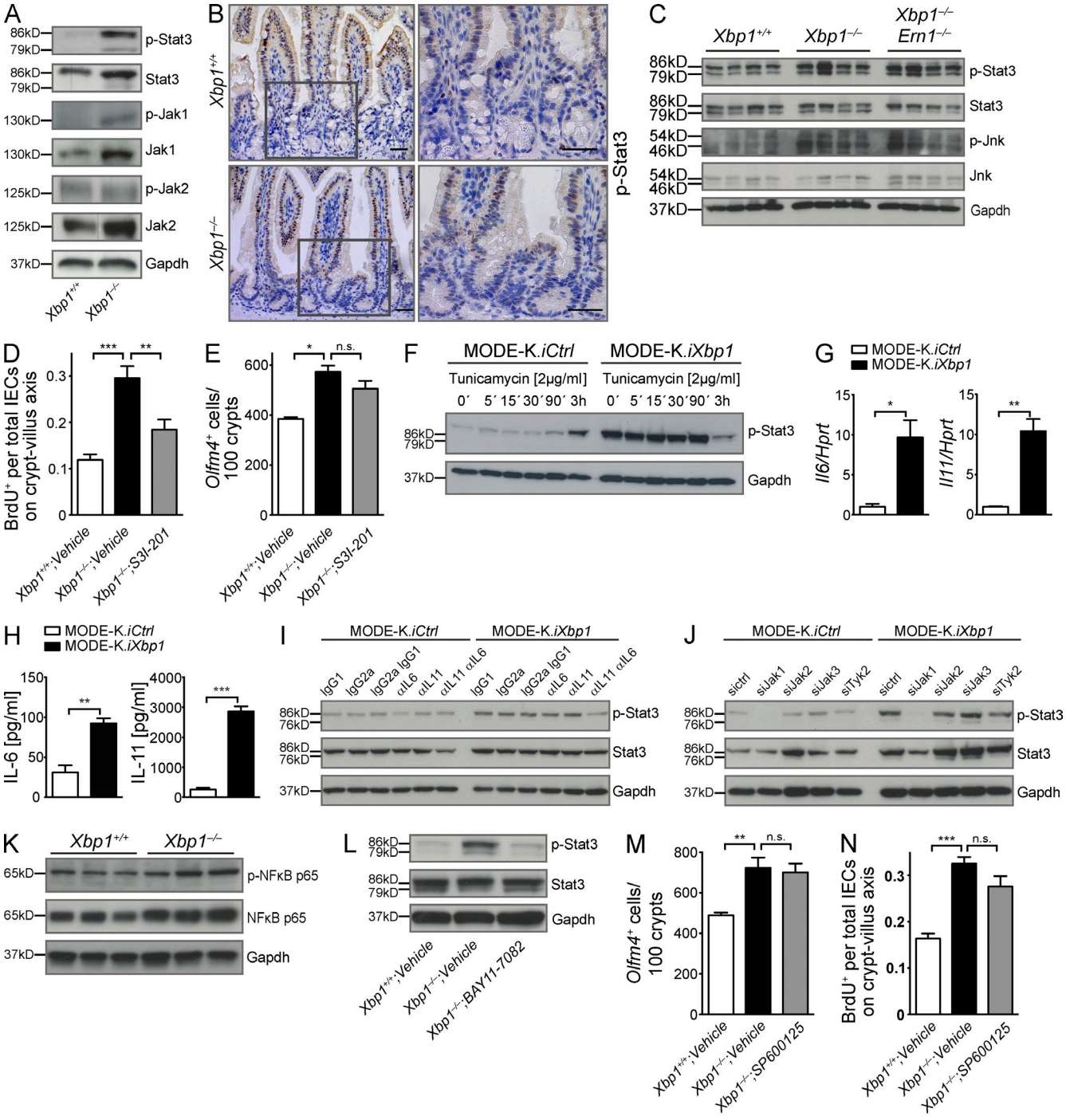

Figure 3. Hypomorphic Xbp1 leads to Jak1/Stat3 activation in the intestinal epithelium. (A) Immunoblot for p-Stat3, Stat3, p-Jak1, Jak1, p-Jak2, and Jak2 on epithelial colonic scrapings. Data are representative of more than four independent experiments. (B) IHC localizes p-Stat3 immunoreactivity to IECs in the transit-amplifying zone and villus, but largely spares the crypt bottom (n = 3/3). Boxed areas are shown at higher magnification on the right. Bars, 20 µm. (C) Small intestinal epithelial scrapings from the indicated genotypes were analyzed for p-Stat3, Stat3, p-Jnk, and Jnk. The experiment was performed with four mice per group. (D) Mice were treated with the Stat3 inhibitor S3I-201 or vehicle for 14 d, and BrdU was administered 24 h before harvest. The ratio of BrdU$^+$ cells per total IECs along the crypt–villus axis in the small intestine is presented (n = 4/5/7; one-way ANOVA with Bonferroni post-hoc test). (E) Olfm4$^+$ ISCs counted in the same experiment as in D (n = 2/3/3; one-way ANOVA with Bonferroni post-hoc test). (F) MODE-K.*iXbp1* and MODE-K.*iCtrl* cells were stimulated with the ER stress inducer tunicamycin and analyzed for Stat3 Tyr-705 phosphorylation. Data are representative of two independent experiments. (G) *Il6* and *Il11* mRNA expression in MODE-K.*iXbp1* and MODE-K.*iCtrl* cells (n = 3; two-sided Student's t test). Data are representative of two independent experiments. (H) Supernatants from MODE-K.*iXbp1* and MODE-K.*iCtrl* cells were analyzed for IL-6 and IL-11 secretion by ELISA (n = 6; two-sided Student's t test). (I) MODE-K.*iXbp1* and MODE-K.*iCtrl* cells were incubated with anti–IL-11 and anti–IL-6 mAbs or respective

control-silenced cells (Fig. 3 F). Stat3 Tyr-705 phosphorylation was also induced in *Xbp1*-sufficient MODE-K cells after ER stress induction via tunicamycin (Fig. 3 F). The extent of Stat3 phosphorylation in *Xbp1*-silenced MODE-K cells was not further augmented by incubation with tunicamycin (Fig. 3 F) and, in fact, decreased at the latest time point studied, likely reflecting the exhaustion of the compensatory UPR (Fig. 3 F). These experiments establish that Stat3 activation in IECs is likely to be an IEC-intrinsic consequence of unresolved ER stress.

IL-6 and IL-11 are prototypical Stat3-activating cytokines (Yu et al., 2009). *Xbp1* silencing induced mRNA expression and protein secretion of IL-6 and IL-11 in MODE-K cells (Fig. 3, G and H). Neutralization experiments with anti-cytokine antibodies revealed that combined administration of anti–IL-6 and anti–IL-11 mAbs abrogated increased Stat3 phosphorylation in MODE-K.*iXbp1* cells (Fig. 3 I). Co-silencing of individual cytokine receptor–associated Janus tyrosine kinases (Jak1-3 and Tyk2; Yu et al., 2009) in MODE-K.*iXbp1* cells revealed Jak1 as the critical kinase for Stat3 activation under ER stress conditions (Fig. 3 J). These data indicate that hypomorphic Xbp1 leads to induction of IL-6 and IL-11 secretion in IECs, which in turn activates Stat3 phosphorylation via a Jak1-dependent mechanism.

Il6 is typically transactivated by NF-κB (and, e.g., also by Stat3; Vallabhapurapu and Karin, 2009; Yu et al., 2009). ER stress can lead to NF-κB activation via several mechanisms (Vallabhapurapu and Karin, 2009). $Xbp1^{-/-(IEC)}$ IECs exhibited increased total NF-κB p65 and p-p65 compared with $Xbp1^{+/+(IEC)}$ mice (Fig. 3 K). Blocking NF-κB activation in $Xbp1^{-/-(IEC)}$ mice via the specific irreversible inhibitor of IκBα phosphorylation, BAY 11-7082 (Pierce et al., 1997), indeed abrogated Stat3 activation to baseline levels observed in $Xbp1^{+/+(IEC)}$ littermates (Fig. 3 L). Hence, hypomorphic Xbp1 function is associated with increased NF-κB–dependent activation of Stat3 in IECs.

Jnk inhibition in $Xbp1^{-/-(IEC)}$ mice does not affect ISC expansion or hyperproliferation

Hypomorphic Xbp1 function had previously been reported to result in activation of Jnk, and pharmacological blockade of Jnk phosphorylation with the specific inhibitor SP600125 resulted in abrogation of elevated CXCL1 secretion in *Xbp1*-deficient IECs (Kaser et al., 2008). Biteau et al. (2008) reported that Jnk regulates proliferation and the regenerative capacity of somatic stem cells in the *Drosophila* gut. Moreover, Jnk can be recruited to Ire1 via the adapter molecule tumor necrosis factor receptor–associated factor 2 (Traf2) under certain conditions of ER stress (Urano et al., 2000). To test the hypothesis that Jnk activation may contribute to the Ire1α-dependent increase in ISC numbers or has a role in determining the increased proliferative output of the transit-amplifying zone, we administered SP600125 i.p. every other day for 14 d to $Xbp1^{-/-(IEC)}$ mice. As depicted in Fig. 3 (M and N), SP600125 affected neither Olfm4$^+$ ISC numbers nor IEC turnover along the crypt–villus axis. Furthermore, increased Jnk phosphorylation in IECs was indistinguishable between $Xbp1^{-/-(IEC)}$;$Ern1^{-/-(IEC)}$ and $Xbp1^{-/-(IEC)}$ mice and hence not under the control of Ire1α (Fig. 3 C). These observations let us conclude that Jnk does not have a critical role in the hyperregenerative phenotype observed in the ER-stressed, *Xbp1*-deficient intestine.

Xbp1 protects from CAC

Long-standing IBD may lead to CAC, which has served as a paradigm for the relationship between inflammation and cancer (Grivennikov et al., 2010; Mantovani, 2010; Danese and Fiocchi, 2011). The mediators involved in regeneration of the ER-stressed, *Xbp1*-deficient intestinal epithelium, such as Stat3, IL-6/IL-11, and NF-κB, also cooperate to drive CAC (Becker et al., 2004; Greten et al., 2004; Bollrath et al., 2009; Grivennikov et al., 2009; Grivennikov and Karin, 2010; Kuraishy et al., 2011). We therefore induced CAC by azoxymethane (AOM), followed by three cycles of dextran sodium sulfate (DSS; Fig. 4 A; Greten et al., 2004). $Xbp1^{-/-(IEC)}$ mice developed >10-fold more and larger colonic tumors compared with $Xbp1^{+/+(IEC)}$ littermate controls (Fig. 4, B–D). When analyzed at an early time point (day 15 after initiation), atypical regenerative lesions were only detected in $Xbp1^{-/-(IEC)}$, but not in $Xbp1^{+/+(IEC)}$, mice (Fig. 4 E). Similarly, reactive oxygen species (ROS) levels were increased fivefold in $Xbp1^{-/-(IEC)}$ relative to $Xbp1^{+/+(IEC)}$ epithelia at day 15 (Fig. 4 F), consistent with ROS generation in ER-stressed, *Xbp1*-deficient cells (Liu et al., 2009) and increased severity of DSS colitis in $Xbp1^{-/-(IEC)}$ mice (Kaser et al., 2008). ROS can lead to DNA damage and thereby contribute to cancer initiation and progression (Sedelnikova et al., 2010). Indeed, at day 15, $Xbp1^{-/-(IEC)}$ epithelia exhibited nuclear staining for p53 (Fig. 4 E), evidence for a DNA damage response (Brady et al., 2011), together with a trend toward an increase in aneuploid cells compared

isotype control antibodies, and Stat3 Tyr-705 phosphorylation was analyzed in cell lysates. Data are representative of three independent experiments. (J) MODE-K.*iXbp1* and MODE-K.*iCtrl* cells were co-silenced with *Jak1*-, *Jak2*-, *Jak3*-, and *Tyk2*-specific or scrambled siRNAs, and Stat3 Tyr-705 phosphorylation was analyzed. Data are representative of four independent experiments. (K) IECs of $Xbp1^{+/+(IEC)}$ and $Xbp1^{-/-(IEC)}$ mice were analyzed for p–NF-κB p65 and total NF-κB p65. Data are representative of two independent experiments. (L) The NF-κB inhibitor BAY 11-7082 or vehicle was administered to $Xbp1^{+/+(IEC)}$ and $Xbp1^{-/-(IEC)}$ mice for 2 wk, and Stat3 Tyr-705 phosphorylation was analyzed in small IEC scrapings. Data are representative of three independent experiments. (A, C, F, and I–L) Gapdh was used as a loading control. (M) Mice were treated with the Jnk inhibitor SP600125 or vehicle for 14 d, and Olfm4$^+$ ISCs were counted (n = 5/6/7; one-way ANOVA with Bonferroni post-hoc test). (N) The ratio of BrdU$^+$ cells per total IECs along the crypt–villus axis in the small intestine 24 h after BrdU administration is analyzed in the same experiment as in M (n = 5/6/7; one-way ANOVA with Bonferroni post-hoc test). Graphs show mean ± SEM. *, P < 0.05; **, P < 0.01; ***, P < 0.001.

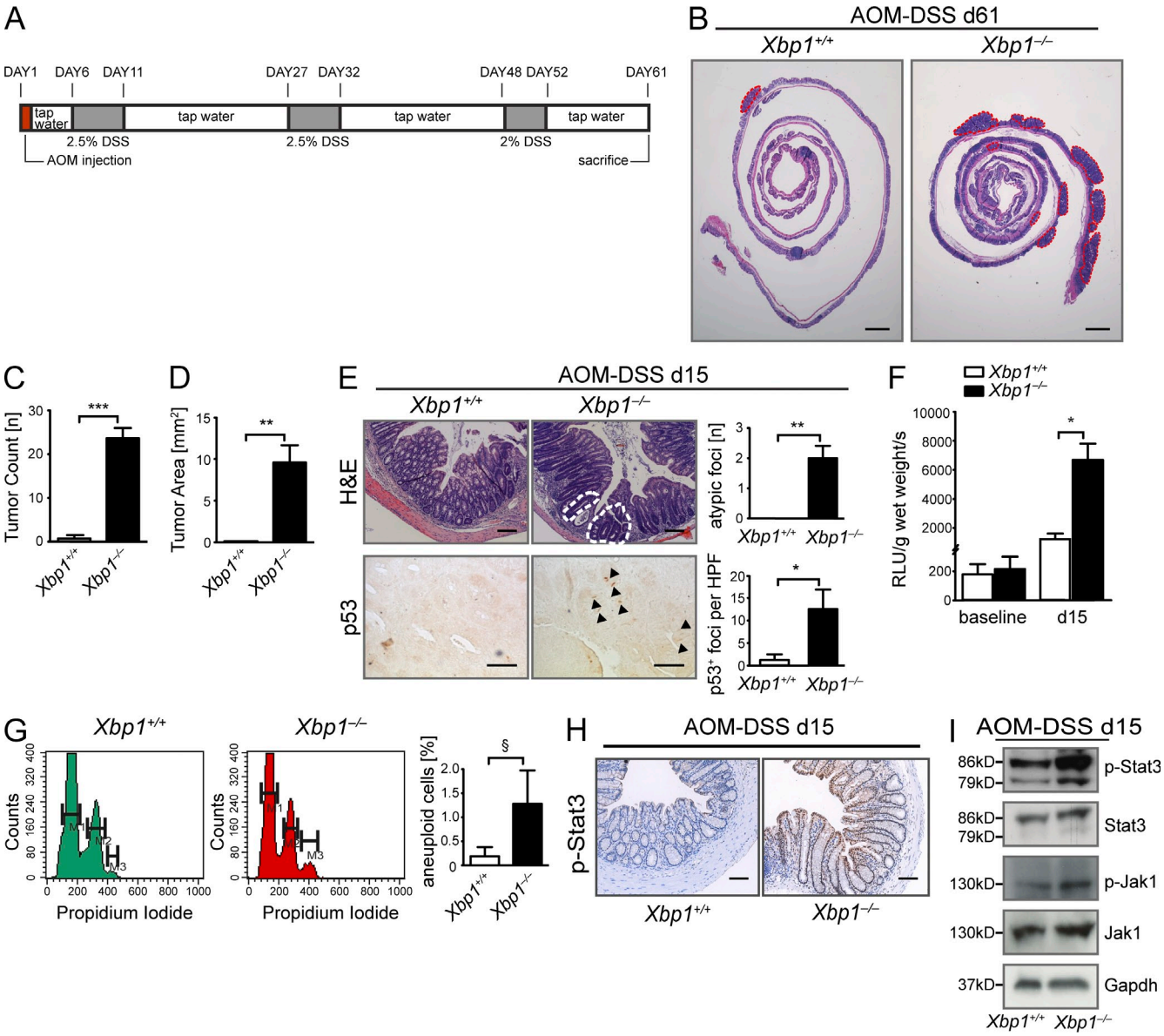

Figure 4. Xbp1 suppresses CAC. (A) Schematic overview of the AOM/DSS CAC model. (B) Representative H&E staining of colon of $Xbp1^{+/+(IEC)}$ and $Xbp1^{-/-(IEC)}$ at day 61 of AOM/DSS colitis. Individual tumors are highlighted by red dashed lines (one of three individual experiments; $n = 4/3$; total $n = 13/10$). (C and D) Tumor number (C) and area (D) in $Xbp1^{+/+(IEC)}$ and $Xbp1^{-/-(IEC)}$ at day 61 of AOM/DSS colitis (one of three individual experiments; $n = 4/3$; total $n = 13/10$; two-sided Student's t test). (E, top) Atypical regenerative foci (white dashed lines) identified on H&E stainings on day 15 of AOM/DSS colitis. Number of lesions per colon is shown. (bottom) Staining for p53 was analyzed by IHC (arrowheads, $p53^+$ nuclei; HPF, high power field; $n = 4/4$; two-sided Student's t test). (F) ROS in colonic epithelium before ($n = 6/7$; two-sided Student's t test) and on day 15 of AOM/DSS ($n = 5/5$; two-sided Student's t test). (G) Detection of aneuploidy by analysis of DNA content with propidium iodide in isolated colonic IECs ($n = 3/3$; one-sided Student's t test; M1 = G_0/G_1; M2 = G_2/S; M3 = aneuploid). (H) IHC on day 15 of the AOM/DSS model localizes increased p-Stat3 immunoreactivity to IECs ($n = 4/4$). Bars: (B) 2 mm; (E [top] and H) 50 µm; (E, bottom) 20 µm. (I) Western blot for p-Stat3, Stat3, p-Jak1, and Jak1 on colonic IEC scrapings on day 15 of the AOM/DSS model. Gapdh was used as a loading control. Data are representative of two independent experiments. Graphs show mean ± SEM. §, $P = 0.1024$; *, $P < 0.05$; **, $P < 0.01$; ***, $P < 0.001$.

with $Xbp1^{+/+(IEC)}$ IECs (Fig. 4 G). Moreover, Stat3 phosphorylation was increased in $Xbp1^{-/-(IEC)}$ compared with $Xbp1^{+/+(IEC)}$ mice (Fig. 4, H and I). These observations imply that epithelial *Xbp1* deficiency is associated with a profound increase in tumorigenesis in CAC. Because IEC-specific *Xbp1* deficiency is associated with increased severity of DSS-induced colitis (Kaser et al., 2008), increased tumorigenesis in $Xbp1^{-/-(IEC)}$ compared with $Xbp1^{+/+(IEC)}$ mice in the AOM/DSS model as observed here may result from a combination of inflammatory, tumor-promoting signals emanating from the more intense myeloid infiltrate (Greten et al., 2004; Bollrath et al., 2009; Grivennikov et al., 2009), as well as from IEC-intrinsic mechanisms.

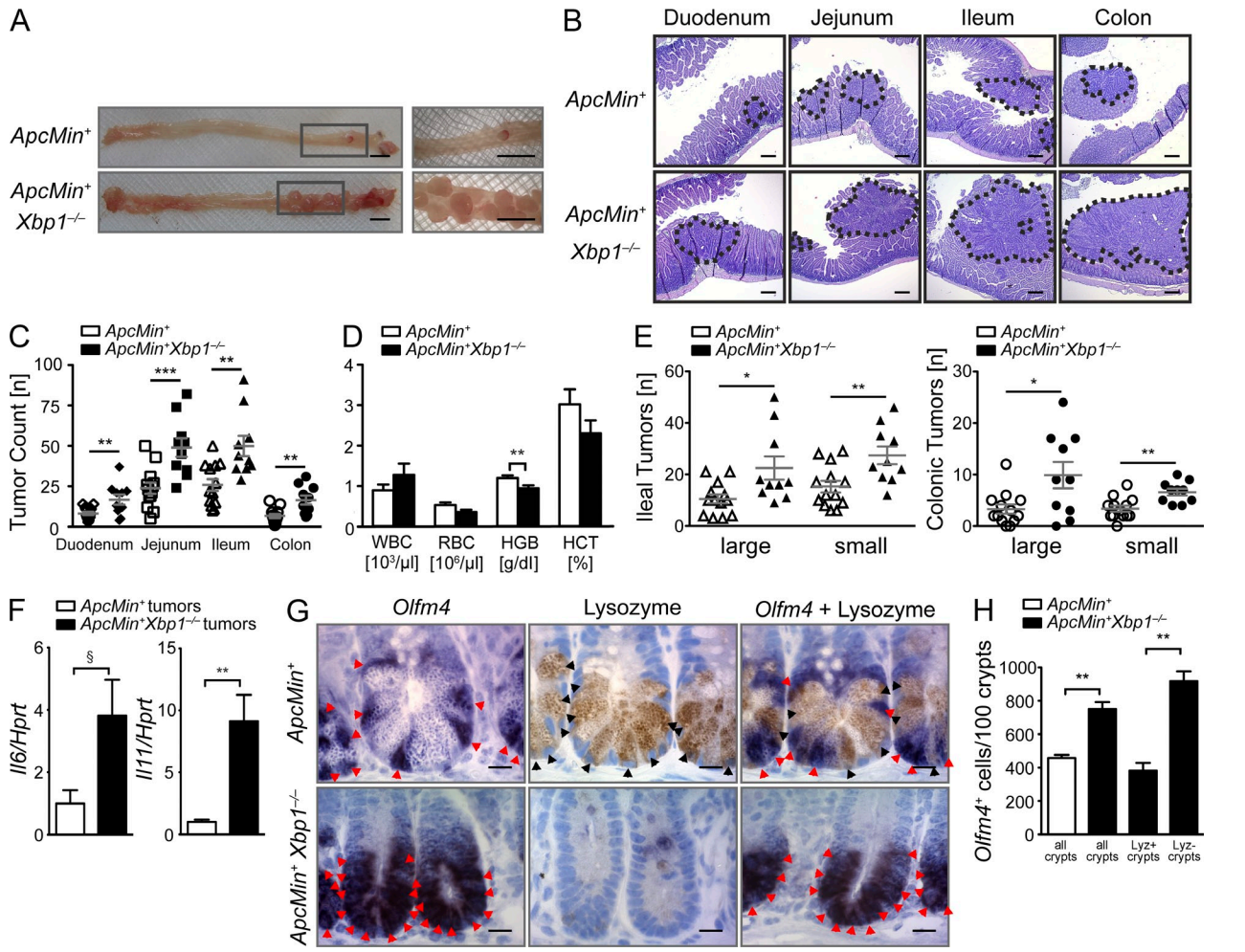

Figure 5. Epithelial Xbp1 suppresses tumor burden in *Apc*^{min} mice. (A) Representative macroscopic pictures of the colon with rectal tumors in the indicated genotypes analyzed at age 15 wk (n = 13/10). Boxed areas are shown at higher magnification on the right. (B) Representative H&E-stained sections, with tumors highlighted by dotted lines (n = 13/10). (C) Quantification of tumor numbers per mouse along the intestinal tract (n = 13/10; two-sided Student's t test). (D) Peripheral blood count of the indicated genotypes at age 15 wk (n = 13/10; two-sided Student's t test). (E) Ileal and colonic tumor counts in the indicated genotypes stratified by size of tumors (n = 13/10; two-sided Student's t test). (F) Tumors from colons of *Xbp1*$^{+/+(IEC)}$;*Apc*^{min} and *Xbp1*$^{-/-(IEC)}$;*Apc*^{min} mice were microdissected, and mRNA expression of the indicated targets was analyzed by qPCR (n = 5/5; two-tailed Student's t test). (G) Olfm4$^+$ ISCs (red arrowheads; ISH) and lysozyme$^+$ Paneth cells (black arrowheads; IHC) in the indicated genotypes (n = 4/4). Bars: (A) 5 mm; (B) 100 µm; (G) 5 µm. (H) Number of Olfm4$^+$ ISCs per 100 crypts in *Xbp1*$^{+/+(IEC)}$;*Apc*^{min} and *Xbp1*$^{-/-(IEC)}$;*Apc*^{min} small intestines. The occasional presence of crypts with lysozyme$^+$ mature Paneth cells among the vast majority of crypts with lysozyme$^-$ Paneth cell remnants in *Xbp1*$^{-/-(IEC)}$;*Apc*^{min} mice allowed crypt-specific stratification of Olfm4$^+$ cell enumeration in lysozyme$^+$ and lysozyme$^-$ crypts (n = 4/4; two-sided Student's t test). Graphs show mean ± SEM. §, P = 0.0519; *, P < 0.05; **, P < 0.01; ***, P < 0.001.

Epithelial Xbp1 suppresses tumor formation in *Apc*$^{min/+}$ mice

Inflammatory signaling is an important contributor to CAC but also to sporadic and familial CRC (Rakoff-Nahoum and Medzhitov, 2007; Lee et al., 2010), with overlapping and distinct inflammatory pathways being involved (Salcedo et al., 2010). ER stress in various organs, including the liver, skeletal muscle, adipose tissue (Ozcan et al., 2004; Gregor et al., 2009; Kars et al., 2010), and intestinal crypts (Hodin et al., 2011), is associated with obesity, which is epidemiologically closely associated with increased cancer incidence, most notably CRC (Calle et al., 2003). CRC and CAC exhibit distinguishing features with regard to their molecular genetic underpinning; e.g., inactivating somatic mutations in *adenomatous polyposis coli* (*APC*) are very common and appear early as a rate-limiting step in CRC pathogenesis (Kinzler and Vogelstein, 1996; Fearon, 2011; Cancer Genome Atlas Network, 2012) but late in CAC (Leedham et al., 2009). Germline mutations in *APC* also cause familial adenomatous polyposis. *APC*-associated CRC can be modeled in *Apc* mutant mice (Moser et al., 1990). Such a model has enabled the determination that ISCs are the cells of origin in CRC (Barker et al., 2009; Zhu et al., 2009; Schepers et al., 2012). The expansion of ISCs in *Xbp1*$^{-/-(IEC)}$ mice, and the desire to delineate the specific tumor-promoting role of *Xbp1* deficiency specifically in IECs, prompted us to

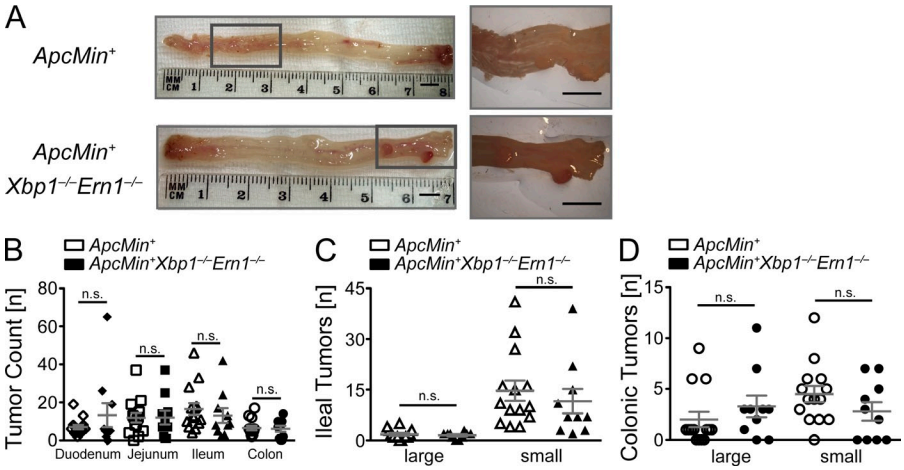

Figure 6. Increased tumor formation in *Xbp1*$^{-/-(IEC)}$;*Apc*^{min} mice is dependent on Ire1α. (A) Representative macroscopic pictures of colonic tumors of the indicated genotypes analyzed at age 15 wk (n = 14/10). Boxed areas are shown at higher magnification on the right. Bars, 5 mm. (B) Enumeration of tumors in the indicated genotypes at 15 wk of age. Mean tumor numbers ± SEM along the intestinal tract are shown (n = 14/10; two-sided Student's t test). (C and D) Ileal (C) and colonic (D) tumor counts stratified by tumor size (n = 14/10; two-sided Student's t test). Graphs show mean ± SEM.

investigate whether unresolved ER stress augments tumorigenesis in this CRC model.

Xbp1$^{-/-(IEC)}$ mice crossed onto an *Apc*^{min} background (*Xbp1*$^{-/-(IEC)}$;*Apc*^{min}) developed twofold more tumors than their *Xbp1*$^{+/+(IEC)}$;*Apc*^{min} littermates (Fig. 5, A–C), along with lower blood hemoglobin levels reflecting intestinal blood loss (Fig. 5 D). Increased tumor numbers in *Xbp1*$^{-/-(IEC)}$;*Apc*^{min} mice were detected in the small intestine, but also the colon, where only few tumors typically develop in the *Apc*^{min} model (Fig. 5, C and E). Colonic tumors are notable because *Xbp1* deletion does not induce colonic, but only small intestinal inflammation (Kaser et al., 2008), suggesting that ER stress–induced tumor promotion is independent of overt inflammation in the colon. Nonetheless, colonic tumors from *Xbp1*$^{-/-(IEC)}$;*Apc*^{min} mice exhibited increased *Il6* and *Il11* mRNA expression compared with those from *Xbp1*$^{+/+(IEC)}$;*Apc*^{min} littermate controls (Fig. 5 F). Tumors in *Xbp1*-deficient mice exhibited *Xbp1* deletion, excluding outgrowth from *Xbp1*-sufficient IECs (not depicted). Together, these experiments demonstrate that Xbp1 suppresses the growth of spontaneously arising intestinal tumors.

ISC expansion is individually determined in each Xbp1-deficient crypt

The *Xbp1*$^{-/-(IEC)}$;*Apc*^{min} model serendipitously also afforded us the opportunity to study whether regulation of ISC numbers by Xbp1 was autonomously regulated within individual crypts or, alternatively, was a consequence of the inflammatory milieu of the inflamed small intestinal mucosa. Although lysozyme staining was absent in the vast majority of Paneth cells (i.e., Paneth cell remnants) in *Xbp1*$^{-/-(IEC)}$ epithelia (Fig. 1 F; Kaser et al., 2008), the occasional (~5%) occurrence of crypts with intact lysozyme$^+$ Paneth cells in *Xbp1*$^{-/-(IEC)}$;*Apc*^{min} epithelia (which is presumably caused by inefficient *Cre*-mediated *Xbp1* deletion and hence mosaicism or, alternatively, caused by effective adaptation to ER stress despite *Xbp1* deletion) allowed us to quantify Olfm4$^+$ ISCs separately in crypts without (i.e., Paneth cell remnants) and with (i.e., normal, mature Paneth cells) lysozyme expression. Within the *Xbp1*$^{-/-(IEC)}$;*Apc*^{min} genotype, ISC expansion was solely noted in crypts with Paneth cell remnants, whereas crypts with intact lysozyme$^+$ Paneth cells (in immediate vicinity to those without) exhibited ISC numbers indistinguishable from those found in the *Xbp1*$^{+/+(IEC)}$;*Apc*^{min} genotype (Fig. 5, G and H). These data suggest that expansion of ISCs is not merely a result of the surrounding proinflammatory milieu, which would similarly affect the occasional crypts with intact lysozyme$^+$ Paneth cells, but an IEC-inherent, Xbp1- and ER stress–dependent, crypt-autonomous process.

Tumor formation in *Xbp1*$^{-/-(IEC)}$;*Apc*^{min} mice is dependent on Ire1α

Analogous to its role in ISC expansion under ER stress, we hypothesized that tumor formation in *Xbp1*$^{-/-(IEC)}$;*Apc*^{min} mice would be dependent on Ire1α. Hence, *Ern1*$^{-/-(IEC)}$;*Xbp1*$^{-/-(IEC)}$;*Apc*^{min} mice would be predicted to be indistinguishable in tumor formation from *Apc*^{min} mice. We generated mice that harbored floxed alleles for both *Xbp1* and *Ern1* that were also hemizygous for *Apc*^{min} and compared littermates that expressed one allele of the *Villin-Cre* transgene with those that did not. We observed that deletion of *Ern1* in the intestinal epithelium eliminated the increased tumorigenesis caused by *Xbp1* deficiency in *Apc*^{min} mice. Specifically, as depicted in Fig. 6 (A–D), tumor numbers in *Ern1*$^{-/-(IEC)}$;*Xbp1*$^{-/-(IEC)}$;*Apc*^{min} mice were indeed no longer significantly different from *Ern1*$^{+/+(IEC)}$;*Xbp1*$^{+/+(IEC)}$;*Apc*^{min} mice, and even tended to be lower. These data indicate that increased tumor formation in *Apc*^{min} mice consequent to *Xbp1* deletion is dependent on ER stress sensed by Ire1α and may, by inference, be related to the Ire1α-dependent activation of ISCs.

DISCUSSION

We report here that epithelial injury resulting from ER stress is a potent activator of IEC regeneration and promotes intestinal tumorigenesis. Hypomorphic Xbp1 causes ER stress that is sensed by Ire1α and increases ISC numbers, whereas Stat3 signaling, independent of Ire1α, increases the output of differentiated IECs. This organ-protective function, when

sustained, augments tumor formation in both an inflammatory (i.e., CAC after DSS/AOM) and noninflammatory (i.e., CRC in *Apc^{min}* mice) context. Cytokines and other factors originating from the more prominent inflammatory infiltrate in *Xbp1$^{-/-(IEC)}$* mice exposed to DSS (Kaser et al., 2008) will likely contribute to increased tumorigenesis in the AOM/DSS CAC model (Kuraishy et al., 2011) through effects on the Ire1α-dependent and -independent pathways described here. However, it is clear that the hyperregenerative response observed in the setting of hypomorphic epithelial Xbp1 function is not only a consequence of increased inflammation as increases in colonic tumor formation were observed in *Apc^{min};Xbp1$^{-/-(IEC)}$* mice, which is not associated with appreciable inflammation in this locale when *Xbp1* is deficient (Kaser et al., 2008). Moreover, increased tumor formation in *Xbp1*-deficient *Apc^{min}* mice is dependent on Ire1α, linking ER stress sensing to increased intestinal tumorigenesis. This relationship has important ramifications as the UPR integrates microbial, environmental, and inflammatory signals at the mucosal surface and highlights an unexpected tumor-suppressive role of Xbp1 that is associated with the intestinal epithelium.

The UPR transcription factor Xbp1 is critical for IEC homeostasis in that its reduced function causes pathological ER stress and spontaneous enteritis in the small intestine (Kaser et al., 2008). As shown here, sensing of unresolved ER stress by Ire1α and its consequent overactivation is centrally related to increased ISC numbers observed in the *Xbp1*-deficient epithelium. Moreover, Ire1α does not notably affect homeostatic ISC function, but is only engaged as part of the regenerative response consequent to pathological ER stress. It might be speculated that this could involve regulated Ire1-dependent decay (RIDD) of mRNAs of as yet poorly defined proteins involved in restraining the ISC niche (e.g., Wnt or growth factor receptor antagonists or regulatory microRNAs [Upton et al., 2012]). RIDD is engaged upon pathological ER stress and results in endonucleolytic degradation of ER-localized mRNAs (Han et al., 2009; Hollien et al., 2009).

Paneth cells secrete factors that support the proliferation of intermingled ISCs (Sato et al., 2011). Paneth cells are particularly susceptible to impairment in the UPR as *Xbp1* deletion in IECs results in loss of their characteristic secretory granules (resulting in Paneth cell remnants); however, Paneth cell remnants remain juxtaposed to ISCs (Kaser et al., 2008). The direct relationship between ISC expansion and the presence of Paneth cell remnants within discrete crypts observed in the *Xbp1$^{-/-(IEC)}$;Apc^{min}* genotype (Fig. 5 H) also implies that ISC expansion may be autonomously regulated within individual crypts. *Xbp1* splicing (i.e., active Xbp1s) localizes to Paneth cells, transit-amplifying cells, and cells further up the crypt–villus axis, whereas ISCs do not express appreciable levels of *Xbp1s* (Heijmans et al., 2013; Schwitalla et al., 2013), raising the possibility that ER stress in Paneth cell remnants may directly promote ISC expansion (Sato et al., 2011). Increased expression of the Paneth cell–specific (Sato et al., 2011) transcript *Wnt11* in *Xbp1$^{-/-(IEC)}$* compared with *Xbp1$^{+/+(IEC)}$* crypts may have a role as a trans-acting factor and deserves further exploration in vivo. Wnt11 has been shown to be expressed at elevated levels in patients with ulcerative colitis (You et al., 2008), gastric carcinoma cell lines, and primary CRC cells (Uysal-Onganer and Kypta, 2012), and it can induce the proliferation and transformation of the IEC6 line in vitro (Ouko et al., 2004). Analogous to the model proposed in this paper, Paneth cells have recently been reported to sense calorie restriction (via mTORC1) and orchestrate ISC expansion in trans (Yilmaz et al., 2012). However, because *Vil-Cre* recombines in all IEC types (including ISCs), another possibility is that the effects of *Xbp1* deletion could also have yet-to-be-defined direct effects on ISCs themselves. However, ISCs express only minute levels of *Xbp1* and do not exhibit evidence of *Xbp1* splicing (Heijmans et al., 2013; Schwitalla et al., 2013) under basal conditions. Neither of these hypotheses are mutually exclusive.

Although expansion of ISCs in the setting of ER stress was mediated by Ire1α, the increased turnover of *Xbp1*-deficient IECs was independent of Ire1α, suggesting different underlying mechanisms for both aspects of this regenerative response. An analogous discordant regulation of ISC expansion and proliferative output from transit-amplifying cells, and hence the engagement of separate mechanisms, has also been observed in the aforementioned study by Yilmaz et al. (2012), in which sensing of calorie restriction via mTORC1 in Paneth cells led to increased ISC numbers but decreased proliferative output of differentiated epithelial cells. IEC-specific Stat3 is essential for epithelial restitution and wound healing upon injury, where it localizes with increased epithelial proliferation (Pickert et al., 2009). Indeed, *Xbp1* deletion, independently of Ire1α, leads to activation of Stat3 in the transit-amplifying zone. Consistent with this, pharmacologic blockade of Stat3 signaling abrogates heightened turnover of IECs in *Xbp1$^{-/-(IEC)}$* mice. The secretion of the Stat3-activating cytokines IL-6 and IL-11 by *Xbp1*-silenced MODE-K cells suggests a feed forward loop instigated by ER-stressed IECs, which is relayed via Jak1. *Il6* is a prototypical NF-κB target gene (Vallabhapurapu and Karin, 2009; Yu et al., 2009), and *Il6* and *Il11* can be transactivated by Stat3 (Yu et al., 2009). Given our observations here, it might be speculated that increased NF-κB activation as a consequence of pathological ER stress (Wu et al., 2004; Schröder and Kaufman, 2005) in the *Xbp1*-deficient epithelium might be an inciting event that leads to excessive production of IL-6, which activates Stat3, which may further transactivate *Stat3*, *Il6*, and *Il11*. Indeed, pharmacologic blockade of NF-κB signaling abrogated Stat3 Tyr-705 phosphorylation in *Xbp1$^{-/-(IEC)}$* epithelium.

Malignant cells are commonly exposed to hypoxia, nutrient deprivation, and pH changes that impact protein folding (Ma and Hendershot, 2004; Hetz et al., 2011; Luo and Lee, 2013). Human tumor cells indeed exhibit evidence of ER stress, and reduced capacity to elicit an UPR within malignant cells results in decreased tumorigenesis in model systems (Ma and Hendershot, 2004; Bi et al., 2005; Fu et al., 2008; Luo and Lee, 2013). Xbp1 has been considered protumorigenic

(Luo and Lee, 2013); Xbp1-deficient tumor cells exhibit impaired growth when xenografted into *Scid* mice (Romero-Ramirez et al., 2004, 2009), and disruption of Ire1/Xbp1 signaling may be exploited pharmacologically for the treatment of multiple myeloma (Lee et al., 2003; Mimura et al., 2012). Our data imply an unexpected tumor-preventive role of Xbp1 in the intestinal epithelium. In this rapidly renewing tissue that is constantly exposed to noxious stimuli that may impact protein folding, Xbp1 may not only assist in resolving ER stress but may thereby keep the regenerative response, including stem cell activation, in check. However, overwhelming the remedial abilities of Xbp1 (e.g., through genetic hypofunction of Xbp1 or persistence of microbial or environmental ER stressors including those that inhibit Xbp1 function; Tashiro et al., 2007) may initiate a compensatory regenerative response, which is facilitative of neoplasias if persistent. In line with this, the architecture of ISCs in close proximity to Paneth cells is preserved in tumors (Schepers et al., 2012), which we speculate might result in a situation in which the increase in ISCs and proliferative output in $Xbp1^{-/-(IEC)}$ tumors may outcompete any potential survival disadvantage of differentiated epithelial cells caused by *Xbp1* deficiency.

Finally, the very mechanisms that appear critical for tumor initiation and promotion during CAC (NF-κB, IL-6, and Stat3; Becker et al., 2004; Greten et al., 2004; Bollrath et al., 2009; Grivennikov et al., 2009, 2010; Kuraishy et al., 2011) are engaged when Xbp1 function is relatively insufficient. In parallel, the Ire1α-dependent expansion of the ISC compartment increases the stochastic chance for genotoxic damage in these cells of origin of intestinal cancer (Barker et al., 2009; Zhu et al., 2009; Medema and Vermeulen, 2011; Schepers et al., 2012). Indeed, the Ire1α dependence of increased tumorigenesis in $Xbp1^{-/-(IEC)};Apc^{min}$ mice critically implies a fundamental role of ER stress sensing as a facilitator of CRC. Apart from integrating environmental, microbial, genetic, and inflammatory inputs that affect ER stress levels at the hostile intestinal surface, Ire1α itself might also be affected by somatic mutations in tumors. Indeed, it has ranked prominently as carrying driver mutations in a large-scale survey of the human kinase-ome in diverse human tumors (Greenman et al., 2007).

In summary, this study demonstrates an unexpected role of Xbp1 in restraining the development of CAC and noninflammation-associated CRC. These Xbp1-dependent effects mechanistically derive from a role for Xbp1 in regulating the activity of Ire1α, which in turn determines the size of the ISC pool and its propensity to develop intestinal neoplasias when perturbed, and in restraining an IEC-intrinsic inflammatory response that is mediated by NF-κB, IL-6, IL-11, and Stat3, which are directly involved in promoting IEC proliferation and expansion of the transit-amplifying compartment. Together, the unrestrained activity of the Ire1α-regulated ISC compartment and Stat3-mediated hyperproliferation are central to the development of colorectal neoplasia in the presence of hypomorphic Xbp1 function.

MATERIALS AND METHODS

Mice. $Xbp1^{fl/fl};VillinCre$ ($Xbp1^{-/-(IEC)}$) mice have been described previously (Kaser et al., 2008). $Ern1^{fl/fl};VillinCre$, $Xbp1^{fl/fl};Ern1^{fl/fl};VillinCre$, $Xbp1^{fl/fl};VillinCre;Apc^{min}$, and $Ern1^{fl/fl};Xbp1^{fl/fl};VillinCre;Apc^{min}$ mice were generated by intercrossing $Xbp1^{-/-(IEC)}$ mice with Apc^{min} (The Jackson Laboratory; Moser et al., 1990) and $Ern1^{fl/fl}$ mice (Iwawaki et al., 2009). All mice were housed under specific pathogen–free conditions at Innsbruck Medical University, the University of Cambridge, and Harvard Medical School. The mating strategy involved keeping the *Cre* and Apc^{min} alleles hemizygous so that nondeleted or non-Apc^{min} offspring was generated at 50% and hence could be used as littermate controls. Mice were born at a Mendelian ratio, and mice on Apc^{min} background were regularly surveyed for rectal bleeding and general health status. Mouse protocols were approved by the relevant authorities, and all procedures were performed in accordance with institutional guidelines, using gender- and age-matched littermate controls whenever possible. S3I-201 (EMD Millipore), SP600125 (Sigma-Aldrich), and BAY 11-7082 (EMD Millipore) were injected i.p. at 10 mg/kg, 30 mg/kg, and 5 mg/kg, respectively, in 6–8-wk-old mice every other day for 14 d.

Antibodies. Antibodies directed to p-Stat3 (Tyr705; D3A7), Stat3 (79D7), p-Jak1 (Tyr1022/1023), Jak1 (6G4), p-Jak2 (Tyr1007/1008; C80C3), Jak2 (D2E12), p–NF-κB p65 (Ser536; 93H1), NF-κB p65 (D14E12), Gapdh (14C10), Ire1α (14C10; all Cell Signaling Technology), Ire1α (H-190, Santa Cruz Biotechnology, Inc.), p-Ire1α (Ser724; Abcam), anti-lysozyme (Dako), p53 (CM5; Vector Laboratories), DIG (Roche), PCNA (PC10; Thermo Fisher Scientific), IL-6 (MP5-20F3), IL-11 (188520), IgG1 isotype control (43414), and IgG2A isotype control (54447; all R&D Systems) were used.

AOM/DSS model. 6-8-wk-old $Xbp1^{-/-(IEC)}$ and $Xbp1^{+/+(IEC)}$ mice were injected i.p. with 12.5 mg/kg AOM (Sigma-Aldrich). Colitis was induced by two cycles of 2.5% DSS (MP Biomedicals) in drinking water for 5 d, followed by a 16-d tap water period (Fig. 4 A; Greten et al., 2004). The final DSS cycle (2%) was administered for 4 d, followed by a 10-d tap water period. Tumor count and tumor area were determined at day 61 in paraffin-embedded hematoxylin and eosin (H&E)–stained "Swiss rolls." Serial sections every 200 µm were analyzed for tumor number and area using the section with the largest diameter for each individual tumor by Scion Image software (Scion Corporation).

Apc^{min} model. Longitudinally cut formalin-fixed intestines of 15-wk-old $Xbp1^{fl/fl};VCre;Apc^{min}$ or $Ern1^{fl/fl};Xbp1^{fl/fl};VCre;Apc^{min}$ mice were analyzed under a stereomicroscope (SZH-ILLD; Olympus) and categorized according to their size (Lee et al., 2010), complemented by H&E sections of paraffin-embedded Swiss rolls (Rakoff-Nahoum and Medzhitov, 2007). Complete blood count was performed using Vet abc plus$^+$ (Scil animal care company GmbH).

MODE-K cell cultures. MODE-K IECs cultured in DMEM-10 were transduced with *Xbp1*-specific or control shRNA lentiviral vectors as described previously (Kaser et al., 2008), and stable clones were established. 10^5 cells were seeded in 6-well plates overnight and *Jak1-3*, *Tyk2*, or control siRNA (Life Technologies) transfected, and experiments were harvested 68–72 h after transfection. Tunicamycin (Sigma-Aldrich) was added at 2 µg/ml and anti–IL-6/11 antibodies or isotype control antibodies at optimal concentrations of 2 µg/ml and 20 µg/ml, respectively, and IL-6 and IL-11 in supernatants were measured by ELISA (BD and R&D Systems, respectively).

Crypt isolation. Crypt isolation was performed as previously reported (Muñoz et al., 2012). In brief, the small intestine was flushed with cold PBS and cut longitudinally. Subsequent to scraping on ice, which removed most villi, the intestine was cut into 5-mm pieces and incubated for 5 min in 5 mM EDTA/PBS. Pieces were placed in 30 mM EDTA/PBS for 30 min, passed through a 100-µm cell strainer, and centrifuged, RNA was isolated from crypts, and RT-qPCR was performed as described below.

RNA extraction, RT-qPCR, and splicing assay. RNA was isolated by the RNeasy Mini kit (QIAGEN). Total RNA was reverse transcribed with M-MLV RT (Invitrogen), and SYBR-Green (Eurogentec) qPCR was performed using MX-3000 (Agilent Technologies). Target gene expression is expressed as ratio to housekeeping gene expression. Splicing assay was performed as described previously (Kaser et al., 2008). See Table S1 for primer sequences.

Western blotting. Total protein lysates from MODE-K, IEC scrapings, or tissue were prepared in RIPA buffer (50 mM Tris, pH 7.4, 150 mM NaCl, 1% Nonidet P-40, 0.5% sodium deoxycholate, and 0.1% SDS). Equal amounts of lysates containing Laemmli buffer were boiled at 95°C and resolved on 8–12.5% SDS-PAGE, and transferred, and Hybond-P polyvinylidene fluoride membranes (GE Healthcare) were blocked with 5% milk in TBS-T, overnight incubated with primary antibody, detected with HRP-conjugated secondary antibody, and visualized with LumiGLO (Cell Signaling Technology).

Immunoprecipitations. 300 µg of protein lysate was incubated for 1 h with 1 µg anti-Ire1α pAb H-190 and pulled down with Sepharose-A. Pull-downs were washed three times with RIPA buffer and eluted with 2× SDS loading buffer, followed by Western blot analysis.

IHC. Sections were deparaffinized in xylol and dehydrated in ethanol. Antigen retrieval was performed using citrate or EDTA buffer for 15 min at sub-boiling temperature in a microwave, followed by blocking of endogenous peroxidases activity. Primary antibody was incubated overnight at 4°C, and secondary biotinylated antibody was detected with streptavidin-HRP (Vector Laboratories). Sections were developed using a DAB Peroxidase Substrate kit (Vector Laboratories). Images were acquired using an Axio Observer Z.1 and AxioCam MRc5 and analyzed with AxioVision software (release 4.8; all Carl Zeiss).

ISH. DIG-labeled sense and antisense cRNA probes (Gregorieff and Clevers, 2010) from full-length cDNA clones (I.M.A.G.E. Consortium) were hybridized for 48 h at 500 ng/ml and visualized using anti-DIG antibody (Roche).

Aneuploid cell fraction. Extroverted intestines were incubated in sodium hypochlorite solution and minced, and IECs were released by 30-min incubation in 1 mM EGTA/1 mM EDTA on ice (Garrett et al., 2009). Samples were passed through a 70-µm filter, fixed in 70% ethanol, stained with propidium iodide and anti-CD45, and analyzed by FACS gating on the $CD45^-$ IEC fraction with doublets discriminated (FACSCalibur and CellQuestPro; BD).

ROS. Colon pieces (proximal, mid, and distal) were incubated in Luminol Assay buffer (10 mM luminol in 1 mM $CaCl_2$, 5 mM glucose in PBS) for 3 min and luminescence was measured (Garrett et al., 2009). Mean RLU/mean wet tissue weight was calculated.

BrdU incorporation and quantification. 2.5 mg BrdU was injected 2 or 24 h before sacrificing mice (Kaser et al., 2008). $BrdU^+$ cells were revealed by a BrdU staining kit (BD). $BrdU^+$ cells per total cells along the crypt–villus axis were counted in five randomly selected crypt–villus axes per single sample.

Statistical analysis. Mean ± SEM is reported. Statistical significance was calculated using a two-tailed Student's *t* test, and significance was assumed for p-values <0.05. Where more than two groups were compared, one-way ANOVA with Bonferroni's post-hoc testing was performed. Grubbs test was used to identify outliers. Data were analyzed using Excel (Microsoft) and Prism (GraphPad Software) software.

Online supplemental material. Table S1 shows primer sequences used in this study. Online supplemental material is available at http://www.jem.org/cgi/content/full/jem.20122341/DC1.

We are indebted to Drs. Laurie H. Glimcher, Ann-Hwee Lee, and David Ron for thoughtful discussion of the project. We further acknowledge technical support by Barbara Enrich and Ines Brosch.

This work has been supported by the European Research Council (ERC) under the European Community's Seventh Framework Programme (FP7/2007-2013)/ERC Grant agreement number 260961 (to A. Kaser), the National Institute for Health Research Cambridge Biomedical Research Centre (A. Kaser), the Austrian Science Fund and Ministry of Science P21530-B18 and START Y446-B18 (to A. Kaser), Innsbruck Medical University (MFI 2007-407 to A. Kaser), the Addenbrooke's Charitable Trust (L. Niederreiter and A. Kaser), Crohn's in Childhood Research Association (CiCRA; L. Niederreiter and A. Kaser), the German Research Council (DFG) SFB877, B9 (to P. Rosenstiel), National Institutes of Health RO1 grants DK44319, DK51362, DK53056, and DK08819 (to R.S. Blumberg), and the Harvard Digestive Disease Center grant DK034854 (to R.S. Blumberg).

The authors have no conflicting financial interests.

Submitted: 19 October 2012
Accepted: 7 August 2013

REFERENCES

Aggarwal, B.B., R.V. Vijayalekshmi, and B. Sung. 2009. Targeting inflammatory pathways for prevention and therapy of cancer: short-term friend, long-term foe. *Clin. Cancer Res.* 15:425–430. http://dx.doi.org/10.1158/1078-0432.CCR-08-0149

Amcheslavsky, A., J. Jiang, and Y.T. Ip. 2009. Tissue damage-induced intestinal stem cell division in *Drosophila*. *Cell Stem Cell*. 4:49–61. http://dx.doi.org/10.1016/j.stem.2008.10.016

Barker, N., J.H. van Es, J. Kuipers, P. Kujala, M. van den Born, M. Cozijnsen, A. Haegebarth, J. Korving, H. Begthel, P.J. Peters, and H. Clevers. 2007. Identification of stem cells in small intestine and colon by marker gene Lgr5. *Nature*. 449:1003–1007. http://dx.doi.org/10.1038/nature06196

Barker, N., R.A. Ridgway, J.H. van Es, M. van de Wetering, H. Begthel, M. van den Born, E. Danenberg, A.R. Clarke, O.J. Sansom, and H. Clevers. 2009. Crypt stem cells as the cells-of-origin of intestinal cancer. *Nature*. 457:608–611. http://dx.doi.org/10.1038/nature07602

Becker, C., M.C. Fantini, C. Schramm, H.A. Lehr, S. Wirtz, A. Nikolaev, J. Burg, S. Strand, R. Kiesslich, S. Huber, et al. 2004. TGF-beta suppresses tumor progression in colon cancer by inhibition of IL-6 trans-signaling. *Immunity*. 21:491–501. http://dx.doi.org/10.1016/j.immuni.2004.07.020

Bertolotti, A., X. Wang, I. Novoa, R. Jungreis, K. Schlessinger, J.H. Cho, A.B. West, and D. Ron. 2001. Increased sensitivity to dextran sodium sulfate colitis in IRE1beta-deficient mice. *J. Clin. Invest.* 107:585–593. http://dx.doi.org/10.1172/JCI11476

Bi, M., C. Naczki, M. Koritzinsky, D. Fels, J. Blais, N. Hu, H. Harding, I. Novoa, M. Varia, J. Raleigh, et al. 2005. ER stress-regulated translation increases tolerance to extreme hypoxia and promotes tumor growth. *EMBO J.* 24:3470–3481. http://dx.doi.org/10.1038/sj.emboj.7600777

Biteau, B., C.E. Hochmuth, and H. Jasper. 2008. JNK activity in somatic stem cells causes loss of tissue homeostasis in the aging *Drosophila* gut. *Cell Stem Cell*. 3:442–455. http://dx.doi.org/10.1016/j.stem.2008.07.024

Bollrath, J., T.J. Phesse, V.A. von Burstin, T. Putoczki, M. Bennecke, T. Bateman, T. Nebelsiek, T. Lundgren-May, O. Canli, S. Schwitalla, et al. 2009. gp130-mediated Stat3 activation in enterocytes regulates cell survival and cell-cycle progression during colitis-associated tumorigenesis. *Cancer Cell*. 15:91–102. http://dx.doi.org/10.1016/j.ccr.2009.01.002

Brady, C.A., D. Jiang, S.S. Mello, T.M. Johnson, L.A. Jarvis, M.M. Kozak, D. Kenzelmann Broz, S. Basak, E.J. Park, M.E. McLaughlin, et al. 2011. Distinct p53 transcriptional programs dictate acute DNA-damage responses and tumor suppression. *Cell*. 145:571–583. http://dx.doi.org/10.1016/j.cell.2011.03.035

Buczacki, S.J., H.I. Zecchini, A.M. Nicholson, R. Russell, L. Vermeulen, R. Kemp, and D.J. Winton. 2013. Intestinal label-retaining cells are secretory precursors expressing Lgr5. *Nature*. 495:65–69. http://dx.doi.org/10.1038/nature11965

Calle, E.E., C. Rodriguez, K. Walker-Thurmond, and M.J. Thun. 2003. Overweight, obesity, and mortality from cancer in a prospectively studied cohort of U.S. adults. *N. Engl. J. Med.* 348:1625–1638. http://dx.doi.org/10.1056/NEJMoa021423

Cancer Genome Atlas Network. 2012. Comprehensive molecular characterization of human colon and rectal cancer. *Nature*. 487:330–337. http://dx.doi.org/10.1038/nature11252

Clevers, H. 2013. Stem Cells: A unifying theory for the crypt. *Nature*. 495:53–54. http://dx.doi.org/10.1038/nature11958

Cronin, S.J., N.T. Nehme, S. Limmer, S. Liegeois, J.A. Pospisilik, D. Schramek, A. Leibbrandt, R.de.M. Simoes, S. Gruber, U. Puc, et al. 2009. Genome-wide RNAi screen identifies genes involved in intestinal pathogenic bacterial infection. *Science*. 325:340–343. http://dx.doi.org/10.1126/science.1173164

Danese, S., and C. Fiocchi. 2011. Ulcerative colitis. *N. Engl. J. Med.* 365:1713–1725. http://dx.doi.org/10.1056/NEJMra1102942

Durand, A., B. Donahue, G. Peignon, F. Letourneur, N. Cagnard, C. Slomianny, C. Perret, N.F. Shroyer, and B. Romagnolo. 2012. Functional intestinal stem cells after Paneth cell ablation induced by the loss of transcription factor Math1 (Atoh1). *Proc. Natl. Acad. Sci. USA*. 109:8965–8970. http://dx.doi.org/10.1073/pnas.1201652109

Fearon, E.R. 2011. Molecular genetics of colorectal cancer. *Annu. Rev. Pathol.* 6:479–507. http://dx.doi.org/10.1146/annurev-pathol-011110-130235

Fu, Y., S. Wey, M. Wang, R. Ye, C.P. Liao, P. Roy-Burman, and A.S. Lee. 2008. Pten null prostate tumorigenesis and AKT activation are blocked by targeted knockout of ER chaperone GRP78/BiP in prostate epithelium. *Proc. Natl. Acad. Sci. USA*. 105:19444–19449. http://dx.doi.org/10.1073/pnas.0807691105

Garrett, W.S., S. Punit, C.A. Gallini, M. Michaud, D. Zhang, K.S. Sigrist, G.M. Lord, J.N. Glickman, and L.H. Glimcher. 2009. Colitis-associated colorectal cancer driven by T-bet deficiency in dendritic cells. *Cancer Cell*. 16:208–219. http://dx.doi.org/10.1016/j.ccr.2009.07.015

Greenman, C., P. Stephens, R. Smith, G.L. Dalgliesh, C. Hunter, G. Bignell, H. Davies, J. Teague, A. Butler, C. Stevens, et al. 2007. Patterns of somatic mutation in human cancer genomes. *Nature*. 446:153–158. http://dx.doi.org/10.1038/nature05610

Gregor, M.F., L. Yang, E. Fabbrini, B.S. Mohammed, J.C. Eagon, G.S. Hotamisligil, and S. Klein. 2009. Endoplasmic reticulum stress is reduced in tissues of obese subjects after weight loss. *Diabetes*. 58:693–700. http://dx.doi.org/10.2337/db08-1220

Gregorieff, A., and H. Clevers. 2010. In situ hybridization to identify gut stem cells. *Curr. Protoc. Stem Cell Biol.* Chapter 2:Unit 2F.1.

Greten, F.R., L. Eckmann, T.F. Greten, J.M. Park, Z.W. Li, L.J. Egan, M.F. Kagnoff, and M. Karin. 2004. IKKbeta links inflammation and tumorigenesis in a mouse model of colitis-associated cancer. *Cell*. 118:285–296. http://dx.doi.org/10.1016/j.cell.2004.07.013

Grivennikov, S.I., and M. Karin. 2010. Dangerous liaisons: STAT3 and NF-kappaB collaboration and crosstalk in cancer. *Cytokine Growth Factor Rev.* 21:11–19. http://dx.doi.org/10.1016/j.cytogfr.2009.11.005

Grivennikov, S., E. Karin, J. Terzic, D. Mucida, G.Y. Yu, S. Vallabhapurapu, J. Scheller, S. Rose-John, H. Cheroutre, L. Eckmann, and M. Karin. 2009. IL-6 and Stat3 are required for survival of intestinal epithelial cells and development of colitis-associated cancer. *Cancer Cell*. 15:103–113. http://dx.doi.org/10.1016/j.ccr.2009.01.001

Grivennikov, S.I., F.R. Greten, and M. Karin. 2010. Immunity, inflammation, and cancer. *Cell*. 140:883–899. http://dx.doi.org/10.1016/j.cell.2010.01.025

Han, D., A.G. Lerner, L. Vande Walle, J.P. Upton, W. Xu, A. Hagen, B.J. Backes, S.A. Oakes, and F.R. Papa. 2009. IRE1alpha kinase activation modes control alternate endoribonuclease outputs to determine divergent cell fates. *Cell*. 138:562–575. http://dx.doi.org/10.1016/j.cell.2009.07.017

Heazlewood, C.K., M.C. Cook, R. Eri, G.R. Price, S.B. Tauro, D. Taupin, D.J. Thornton, C.W. Png, T.L. Crockford, R.J. Cornall, et al. 2008. Aberrant mucin assembly in mice causes endoplasmic reticulum stress and spontaneous inflammation resembling ulcerative colitis. *PLoS Med*. 5:e54. http://dx.doi.org/10.1371/journal.pmed.0050054

Heijmans, J., J.F. van Lidth de Jeude, B.K. Koo, S.L. Rosekrans, M.C. Wielenga, M. van de Wetering, M. Ferrante, A.S. Lee, J.J. Onderwater, J.C. Paton, et al. 2013. ER stress causes rapid loss of intestinal epithelial stemness through activation of the unfolded protein response. *Cell Rep.* 3:1128–1139. http://dx.doi.org/10.1016/j.celrep.2013.02.031

Hetz, C., F. Martinon, D. Rodriguez, and L.H. Glimcher. 2011. The unfolded protein response: integrating stress signals through the stress sensor IRE1α. *Physiol. Rev.* 91:1219–1243. http://dx.doi.org/10.1152/physrev.00001.2011

Hodin, C.M., F.J. Verdam, J. Grootjans, S.S. Rensen, F.K. Verheyen, C.H. Dejong, W.A. Buurman, J.W. Greve, and K. Lenaerts. 2011. Reduced Paneth cell antimicrobial protein levels correlate with activation of the unfolded protein response in the gut of obese individuals. *J. Pathol.* 225:276–284. http://dx.doi.org/10.1002/path.2917

Hollien, J., J.H. Lin, H. Li, N. Stevens, P. Walter, and J.S. Weissman. 2009. Regulated Ire1-dependent decay of messenger RNAs in mammalian cells. *J. Cell Biol.* 186:323–331. http://dx.doi.org/10.1083/jcb.200903014

Iwawaki, T., R. Akai, S. Yamanaka, and K. Kohno. 2009. Function of IRE1 alpha in the placenta is essential for placental development and embryonic viability. *Proc. Natl. Acad. Sci. USA*. 106:16657–16662. http://dx.doi.org/10.1073/pnas.0903775106

Jiang, H., P.H. Patel, A. Kohlmaier, M.O. Grenley, D.G. McEwen, and B.A. Edgar. 2009. Cytokine/Jak/Stat signaling mediates regeneration and homeostasis in the *Drosophila* midgut. *Cell*. 137:1343–1355. http://dx.doi.org/10.1016/j.cell.2009.05.014

Kars, M., L. Yang, M.F. Gregor, B.S. Mohammed, T.A. Pietka, B.N. Finck, B.W. Patterson, J.D. Horton, B. Mittendorfer, G.S. Hotamisligil, and S. Klein. 2010. Tauroursodeoxycholic acid may improve liver and muscle but not adipose tissue insulin sensitivity in obese men and women. *Diabetes*. 59:1899–1905. http://dx.doi.org/10.2337/db10-0308

Kaser, A., and R.S. Blumberg. 2011. Autophagy, microbial sensing, endoplasmic reticulum stress, and epithelial function in inflammatory bowel disease. *Gastroenterology*. 140:1738–1747. http://dx.doi.org/10.1053/j.gastro.2011.02.048

Kaser, A., A.H. Lee, A. Franke, J.N. Glickman, S. Zeissig, H. Tilg, E.E. Nieuwenhuis, D.E. Higgins, S. Schreiber, L.H. Glimcher, and R.S. Blumberg. 2008. XBP1 links ER stress to intestinal inflammation and confers genetic risk for human inflammatory bowel disease. *Cell*. 134:743–756. http://dx.doi.org/10.1016/j.cell.2008.07.021

Kim, T.H., S. Escudero, and R.A. Shivdasani. 2012. Intact function of Lgr5 receptor-expressing intestinal stem cells in the absence of Paneth cells. *Proc. Natl. Acad. Sci. USA*. 109:3932–3937. http://dx.doi.org/10.1073/pnas.1113890109

Kinzler, K.W., and B. Vogelstein. 1996. Lessons from hereditary colorectal cancer. *Cell*. 87:159–170. http://dx.doi.org/10.1016/S0092-8674(00)81333-1

Kohno, K. 2010. Stress-sensing mechanisms in the unfolded protein response: similarities and differences between yeast and mammals. *J. Biochem.* 147:27–33. http://dx.doi.org/10.1093/jb/mvp196

Kuraishy, A., M. Karin, and S.I. Grivennikov. 2011. Tumor promotion via injury- and death-induced inflammation. *Immunity*. 35:467–477. http://dx.doi.org/10.1016/j.immuni.2011.09.006

Lam, L.T., G. Wright, R.E. Davis, G. Lenz, P. Farinha, L. Dang, J.W. Chan, A. Rosenwald, R.D. Gascoyne, and L.M. Staudt. 2008. Cooperative signaling through the signal transducer and activator of transcription 3 and nuclear factor-kappaB pathways in subtypes of diffuse large B-cell lymphoma. *Blood*. 111:3701–3713. http://dx.doi.org/10.1182/blood-2007-09-111948

Lee, A.H., N.N. Iwakoshi, K.C. Anderson, and L.H. Glimcher. 2003. Proteasome inhibitors disrupt the unfolded protein response in myeloma cells. *Proc. Natl. Acad. Sci. USA*. 100:9946–9951. http://dx.doi.org/10.1073/pnas.1334037100

Lee, S.H., L.L. Hu, J. Gonzalez-Navajas, G.S. Seo, C. Shen, J. Brick, S. Herdman, N. Varki, M. Corr, J. Lee, and E. Raz. 2010. ERK activation drives intestinal tumorigenesis in Apc(min/+) mice. *Nat. Med.* 16:665–670. http://dx.doi.org/10.1038/nm.2143

Leedham, S.J., T.A. Graham, D. Oukrif, S.A. McDonald, M. Rodriguez-Justo, R.F. Harrison, N.A. Shepherd, M.R. Novelli, J.A. Jankowski, and N.A. Wright. 2009. Clonality, founder mutations, and field cancerization in human ulcerative colitis-associated neoplasia. *Gastroenterology*. 136:542–550: e6. http://dx.doi.org/10.1053/j.gastro.2008.10.086

Lieberman, D.A. 2009. Clinical practice. Screening for colorectal cancer. *N. Engl. J. Med.* 361:1179–1187. http://dx.doi.org/10.1056/NEJMcp0902176

Liu, Y., M. Adachi, S. Zhao, M. Hareyama, A.C. Koong, D. Luo, T.A. Rando, K. Imai, and Y. Shinomura. 2009. Preventing oxidative stress: a new role for XBP1. *Cell Death Differ.* 16:847–857. http://dx.doi.org/10.1038/cdd.2009.14

Luo, B., and A.S. Lee. 2013. The critical roles of endoplasmic reticulum chaperones and unfolded protein response in tumorigenesis and anticancer therapies. *Oncogene*. 32:805–818. http://dx.doi.org/10.1038/onc.2012.130

Ma, Y., and L.M. Hendershot. 2004. The role of the unfolded protein response in tumour development: friend or foe? *Nat. Rev. Cancer*. 4:966–977. http://dx.doi.org/10.1038/nrc1505

Mantovani, A. 2010. Molecular pathways linking inflammation and cancer. *Curr. Mol. Med*. 10:369–373. http://dx.doi.org/10.2174/156652410791316968

McGovern, D.P., A. Gardet, L. Törkvist, P. Goyette, J. Essers, K.D. Taylor, B.M. Neale, R.T. Ong, C. Lagacé, C. Li, et al; NIDDK IBD Genetics Consortium. 2010. Genome-wide association identifies multiple ulcerative colitis susceptibility loci. *Nat. Genet*. 42:332–337. http://dx.doi.org/10.1038/ng.549

Medema, J.P., and L. Vermeulen. 2011. Microenvironmental regulation of stem cells in intestinal homeostasis and cancer. *Nature*. 474:318–326. http://dx.doi.org/10.1038/nature10212

Mimura, N., M. Fulciniti, G. Gorgun, Y.T. Tai, D. Cirstea, L. Santo, Y. Hu, C. Fabre, J. Minami, H. Ohguchi, et al. 2012. Blockade of XBP1 splicing by inhibition of IRE1α is a promising therapeutic option in multiple myeloma. *Blood*. 119:5772–5781. http://dx.doi.org/10.1182/blood-2011-07-366633

Montgomery, R.K., D.L. Carlone, C.A. Richmond, L. Farilla, M.E. Kranendonk, D.E. Henderson, N.Y. Baffour-Awuah, D.M. Ambruzs, L.K. Fogli, S. Algra, and D.T. Breault. 2011. Mouse telomerase reverse transcriptase (mTert) expression marks slowly cycling intestinal stem cells. *Proc. Natl. Acad. Sci. USA*. 108:179–184. http://dx.doi.org/10.1073/pnas.1013004108

Moser, A.R., H.C. Pitot, and W.F. Dove. 1990. A dominant mutation that predisposes to multiple intestinal neoplasia in the mouse. *Science*. 247:322–324. http://dx.doi.org/10.1126/science.2296722

Muñoz, J., D.E. Stange, A.G. Schepers, M. van de Wetering, B.-K. Koo, S. Itzkovitz, R. Volckmann, K.S. Kung, J. Koster, S. Radulescu, et al. 2012. The Lgr5 intestinal stem cell signature: robust expression of proposed quiescent '+4' cell markers. *EMBO J.* 31:3079–3091. http://dx.doi.org/10.1038/emboj.2012.166

Narimatsu, M., H. Maeda, S. Itoh, T. Atsumi, T. Ohtani, K. Nishida, M. Itoh, D. Kamimura, S.J. Park, K. Mizuno, et al. 2001. Tissue-specific autoregulation of the stat3 gene and its role in interleukin-6-induced survival signals in T cells. *Mol. Cell. Biol*. 21:6615–6625. http://dx.doi.org/10.1128/MCB.21.19.6615-6625.2001

Ouko, L., T.R. Ziegler, L.H. Gu, L.M. Eisenberg, and V.W. Yang. 2004. Wnt11 signaling promotes proliferation, transformation, and migration of IEC6 intestinal epithelial cells. *J. Biol. Chem*. 279:26707–26715. http://dx.doi.org/10.1074/jbc.M402877200

Ozcan, U., Q. Cao, E. Yilmaz, A.H. Lee, N.N. Iwakoshi, E. Ozdelen, G. Tuncman, C. Görgün, L.H. Glimcher, and G.S. Hotamisligil. 2004. Endoplasmic reticulum stress links obesity, insulin action, and type 2 diabetes. *Science*. 306:457–461. http://dx.doi.org/10.1126/science.1103160

Pickert, G., C. Neufert, M. Leppkes, Y. Zheng, N. Wittkopf, M. Warntjen, H.A. Lehr, S. Hirth, B. Weigmann, S. Wirtz, et al. 2009. STAT3 links IL-22 signaling in intestinal epithelial cells to mucosal wound healing. *J. Exp. Med*. 206:1465–1472. http://dx.doi.org/10.1084/jem.20082683

Pierce, J.W., R. Schoenleber, G. Jesmok, J. Best, S.A. Moore, T. Collins, and M.E. Gerritsen. 1997. Novel inhibitors of cytokine-induced IkappaBalpha phosphorylation and endothelial cell adhesion molecule expression show anti-inflammatory effects in vivo. *J. Biol. Chem*. 272:21096–21103. http://dx.doi.org/10.1074/jbc.272.34.21096

Rakoff-Nahoum, S., and R. Medzhitov. 2007. Regulation of spontaneous intestinal tumorigenesis through the adaptor protein MyD88. *Science*. 317:124–127. http://dx.doi.org/10.1126/science.1140488

Romero-Ramirez, L., H. Cao, D. Nelson, E. Hammond, A.H. Lee, H. Yoshida, K. Mori, L.H. Glimcher, N.C. Denko, A.J. Giaccia, et al. 2004. XBP1 is essential for survival under hypoxic conditions and is required for tumor growth. *Cancer Res.* 64:5943–5947. http://dx.doi.org/10.1158/0008-5472.CAN-04-1606

Romero-Ramirez, L., H. Cao, M.P. Regalado, N. Kambham, D. Siemann, J.J. Kim, Q.T. Le, and A.C. Koong. 2009. X box-binding protein 1 regulates angiogenesis in human pancreatic adenocarcinomas. *Transl. Oncol*. 2:31–38.

Ron, D., and P. Walter. 2007. Signal integration in the endoplasmic reticulum unfolded protein response. *Nat. Rev. Mol. Cell Biol*. 8:519–529. http://dx.doi.org/10.1038/nrm2199

Salcedo, R., A. Worschech, M. Cardone, Y. Jones, Z. Gyulai, R.M. Dai, E. Wang, W. Ma, D. Haines, C. O'hUigin, et al. 2010. MyD88-mediated signaling prevents development of adenocarcinomas of the colon: role of interleukin 18. *J. Exp. Med*. 207:1625–1636. http://dx.doi.org/10.1084/jem.20100199

Sangiorgi, E., and M.R. Capecchi. 2008. Bmi1 is expressed in vivo in intestinal stem cells. *Nat. Genet*. 40:915–920. http://dx.doi.org/10.1038/ng.165

Sato, T., J.H. van Es, H.J. Snippert, D.E. Stange, R.G. Vries, M. van den Born, N. Barker, N.F. Shroyer, M. van de Wetering, and H. Clevers. 2011. Paneth cells constitute the niche for Lgr5 stem cells in intestinal crypts. *Nature*. 469:415–418. http://dx.doi.org/10.1038/nature09637

Schepers, A.G., H.J. Snippert, D.E. Stange, M. van den Born, J.H. van Es, M. van de Wetering, and H. Clevers. 2012. Lineage tracing reveals Lgr5+ stem cell activity in mouse intestinal adenomas. *Science*. 337:730–735. http://dx.doi.org/10.1126/science.1224676

Schröder, M., and R.J. Kaufman. 2005. The mammalian unfolded protein response. *Annu. Rev. Biochem*. 74:739–789. http://dx.doi.org/10.1146/annurev.biochem.73.011303.074134

Schwitalla, S., A.A. Fingerle, P. Cammareri, T. Nebelsiek, S.I. Göktuna, P.K. Ziegler, O. Canli, J. Heijmans, D.J. Huels, G. Moreaux, et al. 2013. Intestinal tumorigenesis initiated by dedifferentiation and acquisition of stem-cell-like properties. *Cell*. 152:25–38. http://dx.doi.org/10.1016/j.cell.2012.12.012

Sedelnikova, O.A., C.E. Redon, J.S. Dickey, A.J. Nakamura, A.G. Georgakilas, and W.M. Bonner. 2010. Role of oxidatively induced DNA lesions in human pathogenesis. *Mutat. Res.* 704:152–159. http://dx.doi.org/10.1016/j.mrrev.2009.12.005

Siddiquee, K., S. Zhang, W.C. Guida, M.A. Blaskovich, B. Greedy, H.R. Lawrence, M.L. Yip, R. Jove, M.M. McLaughlin, N.J. Lawrence, et al. 2007. Selective chemical probe inhibitor of Stat3, identified through structure-based virtual screening, induces antitumor activity. *Proc. Natl. Acad. Sci. USA*. 104:7391–7396. http://dx.doi.org/10.1073/pnas.0609757104

Snyder, M., X.Y. Huang, and J.J. Zhang. 2008. Identification of novel direct Stat3 target genes for control of growth and differentiation. *J. Biol. Chem*. 283:3791–3798. http://dx.doi.org/10.1074/jbc.M706976200

Takeda, N., R. Jain, M.R. LeBoeuf, Q. Wang, M.M. Lu, and J.A. Epstein. 2011. Interconversion between intestinal stem cell populations in distinct niches. *Science*. 334:1420–1424. http://dx.doi.org/10.1126/science.1213214

Tashiro, E., N. Hironiwa, M. Kitagawa, Y. Futamura, S. Suzuki, M. Nishio, and M. Imoto. 2007. Trierixin, a novel Inhibitor of ER stress-induced XBP1 activation from Streptomyces sp. 1. Taxonomy, fermentation, isolation and biological activities. *J. Antibiot*. 60:547–553. http://dx.doi.org/10.1038/ja.2007.69

Tian, H., B. Biehs, S. Warming, K.G. Leong, L. Rangell, O.D. Klein, and F.J. de Sauvage. 2011. A reserve stem cell population in small intestine renders Lgr5-positive cells dispensable. *Nature*. 478:255–259. http://dx.doi.org/10.1038/nature10408

Todd, D.J., A.H. Lee, and L.H. Glimcher. 2008. The endoplasmic reticulum stress response in immunity and autoimmunity. *Nat. Rev. Immunol*. 8:663–674. http://dx.doi.org/10.1038/nri2359

Tréton, X., E. Pédruzzi, D. Cazals-Hatem, A. Grodet, Y. Panis, A. Groyer, R. Moreau, Y. Bouhnik, F. Daniel, and E. Ogier-Denis. 2011. Altered endoplasmic reticulum stress affects translation in inactive colon tissue from patients with ulcerative colitis. *Gastroenterology*. 141:1024–1035. http://dx.doi.org/10.1053/j.gastro.2011.05.033

Upton, J.P., L. Wang, D. Han, E.S. Wang, N.E. Huskey, L. Lim, M. Truitt, M.T. McManus, D. Ruggero, A. Goga, et al. 2012. IRE1α cleaves select microRNAs during ER stress to derepress translation of proapoptotic Caspase-2. *Science*. 338:818–822. http://dx.doi.org/10.1126/science.1226191

Urano, F., X. Wang, A. Bertolotti, Y. Zhang, P. Chung, H.P. Harding, and D. Ron. 2000. Coupling of stress in the ER to activation of JNK protein kinases by transmembrane protein kinase IRE1. *Science*. 287:664–666. http://dx.doi.org/10.1126/science.287.5453.664

Uysal-Onganer, P., and R.M. Kypta. 2012. Wnt11 in 2011 - the regulation and function of a non-canonical Wnt. *Acta Physiol. (Oxf.)*. 204:52–64. http://dx.doi.org/10.1111/j.1748-1716.2011.02297.x

Vallabhapurapu, S., and M. Karin. 2009. Regulation and function of NF-kappaB transcription factors in the immune system. *Annu. Rev. Immunol.* 27:693–733. http://dx.doi.org/10.1146/annurev.immunol.021908.132641

Walter, P., and D. Ron. 2011. The unfolded protein response: from stress pathway to homeostatic regulation. *Science.* 334:1081–1086. http://dx.doi.org/10.1126/science.1209038

Wu, S., M. Tan, Y. Hu, J.L. Wang, D. Scheuner, and R.J. Kaufman. 2004. Ultraviolet light activates NFkappaB through translational inhibition of IkappaBalpha synthesis. *J. Biol. Chem.* 279:34898–34902. http://dx.doi.org/10.1074/jbc.M405616200

Yilmaz, O.H., P. Katajisto, D.W. Lamming, Y. Gültekin, K.E. Bauer-Rowe, S. Sengupta, K. Birsoy, A. Dursun, V.O. Yilmaz, M. Selig, et al. 2012. mTORC1 in the Paneth cell niche couples intestinal stem-cell function to calorie intake. *Nature.* 486:490–495.

You, J., A.V. Nguyen, C.G. Albers, F. Lin, and R.F. Holcombe. 2008. Wnt pathway-related gene expression in inflammatory bowel disease. *Dig. Dis. Sci.* 53:1013–1019. http://dx.doi.org/10.1007/s10620-007-9973-3

Yu, H., D. Pardoll, and R. Jove. 2009. STATs in cancer inflammation and immunity: a leading role for STAT3. *Nat. Rev. Cancer.* 9:798–809. http://dx.doi.org/10.1038/nrc2734

Zhao, F., R. Edwards, D. Dizon, K. Afrasiabi, J.R. Mastroianni, M. Geyfman, A.J. Ouellette, B. Andersen, and S.M. Lipkin. 2010. Disruption of Paneth and goblet cell homeostasis and increased endoplasmic reticulum stress in Agr2-/- mice. *Dev. Biol.* 338:270–279. http://dx.doi.org/10.1016/j.ydbio.2009.12.008

Zheng, W., P. Rosenstiel, K. Huse, C. Sina, R. Valentonyte, N. Mah, L. Zeitlmann, J. Grosse, N. Ruf, P. Nürnberg, et al. 2006. Evaluation of AGR2 and AGR3 as candidate genes for inflammatory bowel disease. *Genes Immun.* 7:11–18. http://dx.doi.org/10.1038/sj.gene.6364263

Zhu, L., P. Gibson, D.S. Currle, Y. Tong, R.J. Richardson, I.T. Bayazitov, H. Poppleton, S. Zakharenko, D.W. Ellison, and R.J. Gilbertson. 2009. Prominin 1 marks intestinal stem cells that are susceptible to neoplastic transformation. *Nature.* 457:603–607. http://dx.doi.org/10.1038/nature07589